

Fluid–Mineral Reactions and Melting of Orthopyroxene–Cordierite–Biotite Gneiss in the Presence of H₂O–CO₂–NaCl and H₂O–CO₂–KCl Fluids under Parameters of Granulite-Facies Metamorphism

O. G. Safonov^{a, b, c, *} and S. A. Kosova^a

^a*Institute of Experimental Mineralogy (IEM), Russian Academy of Sciences, Chernogolovka, Moscow oblast, 142432 Russia*

^b*Geological Faculty, Moscow State University, Moscow, 119899 Russia*

^c*Department of Geology, University of Johannesburg, PO Box 524, Auckland Park, 2006, Johannesburg, South Africa*

**e-mail: oleg@iem.ac.ru*

Received October 11, 2016; in final form, December 16, 2016

Abstract—Reactions and partial melting of peraluminous rocks in the presence of H₂O–CO₂–salt fluids under parameters of granulite-facies metamorphism were modeled in experiments on interaction between orthopyroxene–cordierite–biotite–plagioclase–quartz metapelite with H₂O, H₂O–CO₂, H₂O–CO₂–NaCl, and H₂O–CO₂–KCl fluids at 600 MPa and 850°C. Rock melting in the presence of H₂O and equimolar H₂O–CO₂ fluids generates peraluminous (A/CNK¹ > 1.1) melts whose composition corresponds to magnesian calcic or calc–alkaline S-type granitoids. The melts are associated with peritectic phases: magnesian spinel and orthopyroxene containing up to 9 wt % Al₂O₃. In the presence of H₂O–CO₂–NaCl fluid, cordierite and orthopyroxene are replaced by the association of K–Na biotite, Na-bearing gedrite, spinel, and albite. The Na₂O concentrations in the biotite and gedrite are functions of the NaCl concentrations in the starting fluid. Fluids of the composition H₂O–CO₂–KCl induce cordierite replacement by biotite with corundum and spinel and by these phases in association with potassium feldspar at $X_{\text{KCl}} = 0.02$ in the fluid. When replaced by these phases, cordierite is excluded from the melting reactions, and the overall melting of the metapelite is controlled by peritectic reactions of biotite and orthopyroxene with plagioclase and quartz. These reactions produce such minerals atypical of metapelites as Ca–Na amphibole and clinopyroxene. The compositions of melts derived in the presence of salt-bearing fluids are shifted toward the region with A/CNK < 1.1, as is typical of so-called peraluminous granites of type I. An increase in the concentrations of salts in the fluids leads to depletion of the melts in Al₂O₃ and CaO and enrichment in alkalis. These relations suggest that the protoliths of I-type peraluminous granites might have been metapelites that were melted when interacting with H₂O–CO₂–salt fluids. The compositions of the melts can evolve from those with A/CNK > 1.1 (typical of S-type granites) toward those with A/CNK = 1.0–1.1 in response to an increase in the concentrations of alkali salts in the fluids within a few mole percent. Our experiments demonstrate that the origin of new mineral assemblages in metapelite in equilibrium with H₂O–CO₂–salt fluids is controlled by the activities of alkaline components, while the H₂O and CO₂ activities play subordinate roles. This conclusion is consistent with the results obtained by simulating metapelite mineral assemblages by Gibbs free energy minimization (using the PERPE_X software), as shown in log($a_{\text{H}_2\text{O}}$)–log($a_{\text{Na}_2\text{O}}$) and log($a_{\text{H}_2\text{O}}$)–log($a_{\text{K}_2\text{O}}$) diagrams.

DOI: 10.1134/S086959111705006X

INTRODUCTION

As far back as the 1980s, geochemical data, studies of fluid inclusions, and estimates of the activities of fluid components led some researchers to suggest models in which an active role in amphibolite- and granulite-facies metamorphism was played by fluids bearing dissolved salt components (e.g., Touret, 1985; Aranovich et al., 1987). The role of such fluids in high-temperature metamorphic processes was viewed as either a supplementary or even alternative to the then-dominant concept of “carbon dioxide granulite-facies

metamorphism”, i.e., metamorphism with the participation of CO₂-rich fluid (e.g., Newton et al., 1980; Santosh, 1986). Following D.S. Korzhinskii’s theoretical considerations (Korzhinskii, 1962), L.L. Perchuk and his colleagues (Perchuk and Gerya, 1993; Perchuk et al., 1994) have demonstrated that some processes in the course of high-temperature metamorphism are controlled by variations in K and Na activities in the fluids. Among others things, these processes were thought to involve the development of charnockite and enderbite associations after gneisses of various

composition. To identify these processes, these researchers (Perchuk and Gerya, 1993; Perchuk et al., 1994) suggested certain criteria based on interpretations of reaction textures formed by alkali feldspar at contacts between plagioclase and quartz and/or Fe–Mg minerals, with regard for systematic variations in the mineral chemistries in these textures. These criteria were later often employed by several researchers in studying local charnockitization processes (Perchuk et al., 2000; Ravindra-Kumar, 2004; Safonov et al., 2012; Rajesh et al., 2013; Safonov and Aranovich, 2014) and were even successively extended to other mineral assemblages of high-grade metamorphic rocks (Newton, 1995; Newton et al., 1995, 2014; Harlov et al., 1998, 2014; Franz and Harlov, 1998; Nijland et al., 1998; Safonov, 1998; Harlov and Förster, 2002; Touret and Huizenga, 2011; Touret and Nijland, 2013; Korikovskiy and Aranovich, 2010, 2015; Safonov and Aranovich, 2014; Aranovich and Safonov, 2016). These criteria were also applied to prove that fluids involved in metamorphic processes in the middle and lower crust contain various dissolved salts (e.g., Newton, 1995; Newton and Manning, 2010; Newton et al., 2014; Aranovich et al., 2013, 2014). Their principally important components are K, Na, and Ca chlorides, whose presence in granulite-facies metamorphic fluids follows from finds of inclusions of chloride-bearing solutions and brines (i.e., solutions in equilibrium with solid salt phases) in minerals (Srikantappa and Zargar, 2009; Touret and Huizenga, 2011; Touret and Nijland, 2013), intergranular crystalline chlorides (e.g., Markl and Bucher, 1998), and Cl-enriched amphiboles, biotite, apatite, and scapolite in granulites (see review in Aranovich and Safonov, 2016, and references therein).

Experimental data demonstrate that, in contrast to CO₂ and H₂O–CO₂ fluids, aqueous chloride solutions at high *P* and *T* are able to dissolve much of most rock-forming silicate minerals, carbonates, sulfates, phosphates, and fluorides (Newton and Manning, 2010; Manning, 2013; Aranovich et al., 2014; Manning and Aranovich, 2014) and accessory minerals and actively

exchange components with feldspars and micas (Harlov and Melzer, 2002; Harlov, 2011; Tropper et al., 2011, 2013). Chloride-bearing fluids facilitate more efficient transport of U, Th, REE, Rb, and Cs than their transport in H₂O–CO₂ fluids and granite melts (Hansen et al., 2002; Aranovich et al., 2014). Being highly ionized, concentrated (K,Na)Cl–H₂O fluids under pressures higher than 400 MPa and temperatures of 600–900°C are characterized by a much lower water activity (Aranovich et al., 1987, 2013, 2014; Aranovich and Newton, 1997; Shmulovich and Graham, 1996; Manning, 2013; Manning and Aranovich, 2014) and stabilize typical granulite-facies mineral assemblages in equilibrium with such fluids. Under granulite-facies parameters, aqueous salt solutions are immiscible with CO₂ within a broad compositional range (Johnson, 1991; Gilbert et al., 1998; Shmulovich and Graham, 2004; Heinrich, 2007; Aranovich et al., 2010). The onset of their immiscibility results in two equilibrium fluids with a low water activity and with remarkably different mobility in crystalline rocks (Watson and Brenan, 1987; Gilbert et al., 1998). In granulites, this leads to heterogeneous entrapment of brine inclusions together with CO₂ inclusions (Perchuk et al., 2000; Srikantappa and Zargar, 2009; Touret and Huizenga, 2011; Rajesh et al., 2013). A low water activity typical of equilibrium aqueous salt and CO₂ fluids also precludes active melting of quartz–feldspathic assemblages (Aranovich and Newton, 1996; Shmulovich and Graham, 1996; Aranovich et al., 2013, 2014). Furthermore, concentrated supercritical aqueous salt solutions are relatively little soluble in silicic melts generated by anatexis of crustal rocks (Ryabchikov and Hamilton, 1971; Kilink and Burnham, 1972; Webster, 1997; Shmulovich and Graham, 1996). In equilibrium with aluminosilicate melts, chloride components are preferably distributed into the equilibrium aqueous fluid. Therefore, when anatectic melt is generated, the salinity of the equilibrium fluid increases (Shmulovich and Graham, 1996; Manning and Aranovich, 2014). Nevertheless, the solubility of aqueous salt fluids in magmas is a function of the melt composition (e.g., Webster, 1997), which is in turn dependent on the chemical and mineral composition of the precursor rocks.

Thermodynamic properties of aqueous chloride and H₂O–CO₂ fluid were studied in much detail for model systems (Aranovich and Newton, 1997; Shmulovich and Graham, 1996; Newton and Manning, 2010; Aranovich et al., 2010, 2013, 2014; Manning, 2013; Manning and Aranovich, 2014). These data are, however, not always sufficient to characterize the behavior of chloride-bearing fluids at metamorphism and anatexis in complicated fluid–mineral systems, because the model systems are not able to cover the great diversity of possible reactions between mineral assemblages and salt fluid components. Moreover, it is often difficult to carry out thermodynamic simula-

Abbreviations. **Mineral symbols:** *Ab*—albite, *AlS*—Al silicates, *Amph*—amphibole, *An*—anorthite, *Asp*—aspidolite, *Bt*—biotite, *Cor*—corundum, *Cpx*—clinopyroxene, *Crd*—cordierite, *Di*—diopside, *Eas*—eastonite, *En*—enstatite, *Ged*—gedrite, *Grt*—garnet, *Ilm*—ilmenite, *Kfs*—potassium feldspar, *L*—melt, *Mg-Ts*—Mg-Tschermak molecule, *Mag*—magnetite, *NNO*—Ni–NiO oxygen buffer, *Oam*—orthoamphibole, *Ol*—olivine, *Opx*—orthopyroxene, *Or*—orthoclase, *Phl*—phlogopite, *Pl*—plagioclase, *Prg*—pargasite, *Prs*—preiskerite, *Ru*—rutile, *Qtz*—quartz, *San*—sanidine, *Spl*—spinel. **Compositional parameters:** $X_{Mg} = Mg/(Mg + Fe + Mn)$, $X_{Al} = Al/(Si + Al + Ti + Mg + Fe + Mn)$ (for amphiboles, biotite, and orthopyroxene), $X_{Ca} = Ca/(Ca + Na + K)$ (for plagioclase), $X_{Na} = Na/(K + Na)$ (for biotite). **Petrochemical indices:** $A/CNK = Al_2O_3/(K_2O + Na_2O + CaO)$, $A/NK = Al_2O_3/(K_2O + Na_2O)$ (oxide symbols denote their molar quantities), $MALI = K_2O + Na_2O - CaO$ (oxide symbols denote their weight percentages). **Thermodynamic parameters:** a_i is the activity of component *i*, f_i is the fugacity of component *i*.

tions of these reactions because of inaccuracies in the models of solid solutions of Cl-bearing minerals and melts. In view of this, experiments on interaction of aqueous salt and H₂O-CO₂-salt fluids with natural metamorphic rocks provide important supplements to experimental results in model systems. The most detailed experimental information available as of yet was acquired on interaction between chloride-bearing fluids with mafic and intermediate rocks. L.I. Khodrevskaya (2004) has experimentally studied how amphibolite is granitized by chloride solution percolating through this rock at 500 MPa and 750°C. Experiments at 500 MPa and 900°C (Khodrevskaya and Aranovich, 2016) have also demonstrated that the melting of pargasite amphibole interacting with H₂O-NaCl fluid leads to active saturation of the fluid with silicate components but does not result in complete dehydration of the amphibole, even when the NaCl mole fraction in the fluid reaches 0.45. Larikova and Zarskii (2009) have experimentally reproduced reactions forming amphibole and garnet corona structures in metagabbro interacting with H₂O-NaCl fluid at 500 MPa and 600 and 700°C. It has been demonstrated in (Harlov, 2004) that KCl- and NaCl-bearing fluids stabilize assemblages of orthopyroxene and clinopyroxene with alkali feldspar at the sacrifice of biotite and plagioclase in tonalitic biotite gneiss at 1000 MPa and 900°C. These results have later been confirmed by experiments (Safonov et al., 2014a) on interaction of biotite–amphibole tonalitic gneiss with H₂O-CO₂, H₂O-CO₂-KCl, H₂O-CO₂-NaCl, and H₂O-CO₂-(K,Na)Cl fluid at 550 MPa, 750 and 800°C, and CO₂/(CO₂ + H₂O) = 0.5. The experiments have demonstrated certain tendencies in the transformations of the mineral assemblages depending on the concentrations of the salt components and KCl/NaCl ratio of the fluid. For example, interaction of H₂O-CO₂-KCl fluid with rock at 800°C at KCl concentration increased from 0 to 4 mol % results in systematic changes in the synthesized mineral assemblages from the charnockite-like association *Opx* + *Amph* + *Ilm* + *Ti-Mag* + *Pl* first to *Opx* + *Cpx* + *Ilm* to the syenite-like assemblage *Cpx* ± *Bt* + *Kfs* + *Ilm*. An increase in the NaCl concentration stabilizes amphibole in associations with pyroxenes, but associations of clinopyroxene with albite are formed at high NaCl concentrations. These researchers have shown that reactions forming the foregoing mineral assemblages are largely controlled by the activities of alkalis and that the H₂O and CO₂ activities play thereby subordinate roles. They have suggested to numerically simulate these assemblages by Gibbs free energy minimization (Connolly, 2005) and to calculate log(*a*_{H₂O})–log(*a*_{K₂O}) pseudosections. Experiments and thermodynamic simulations have demonstrated that, in spite of the low water activity, reactions involving H₂O-CO₂-salt fluids intensify the melting of tonalitic gneiss and generate melts whose composi-

tions range from potassic rhyolite in the presence of H₂O-CO₂-KCl fluids to trachyte and phonolite in the presence of H₂O-CO₂-(Na,K)Cl and H₂O-CO₂-NaCl fluids.

No experiments have been so far conducted to model interaction between metamorphic rocks of other types and aqueous chloride or H₂O-CO₂-chloride solutions. These experiments are needed to acquire information on possible mineral indicators of the involvement of such fluids in metamorphic processes. In this context, much interest is attracted to mineral assemblages of metapelites, which commonly make up significant volumes in granulite complexes. These assemblages are rich in Al₂O₃, which has a strong affinity to K and Na, and it is thus reasonable to expect that metapelite minerals should actively react with fluid bearing alkali chlorides. Korzhinskii (1962) has predicted how these reactions should proceed. At a relatively low chemical potential of H₂O and elevated activity of K₂O in the fluid, assemblages of minerals with high Al/Si ratios (for example, sillimanite, cordierite, etc.) are replaced by minerals with lower Al/Si ratios (for example, orthopyroxene or olivine). At a higher chemical potential of H₂O, mineral assemblages are stable in which these minerals are in equilibrium with potassium feldspar and biotite. Korzhinskii has not considered the effect of the chemical potential of Na₂O on transformations of metapelite mineral assemblages, neither has not discussed the involvement of alkali components in melting processes.

This publication is largely focused on experimental tests of relations predicted by Korzhinskii (1962). Below we present results of studying fluid–mineral reactions and reactions of partial melting in orthopyroxene–cordierite–biotite–plagioclase–quartz metapelite in the presence of H₂O, H₂O-CO₂, H₂O-CO₂-NaCl, or H₂O-CO₂-KCl fluid at 600 MPa and 850°C. The experiments were aimed at elucidating how do fluid–mineral reactions, the composition of the equilibrium phases, and melting processes depend on KCl and NaCl concentrations in fluid, at constant *T*, *P*, and H₂O/(H₂O + CO₂). Another our goal was to find mineral indicators of interaction between the metapelite and fluid containing alkali chlorides.

EXPERIMENTAL AND ANALYTICAL TECHNIQUES

Starting Materials and Experimental Procedure

The experiments were carried out with a metapelite sample (sample PET-5) from the Bandelierkop Formation in the Southern Marginal Zone of the Limpopo Complex in South Africa. The sample was described in (Safonov et al., 2014b). This is a fine-grained rock made up of cordierite, orthopyroxene, biotite, plagioclase, and quartz (Table 1, Fig. 1). The accessory minerals are sillimanite, spinel, ilmenite,

apatite, monazite, zircon, pyrrhotite, pentlandite, and chalcopyrite. Although the rock is massive and does not show any clearly seen directional textural features, it is heterogeneous and consists of two types of mineral microassociations: (1) “tonalitic” associations, whose plagioclase commonly occurs with biotite and quartz, and (2) “pelitic” associations, which consist of cordierite and aluminous orthopyroxene. The “pelitic” associations compose equant clusters of orthopyroxene–cordierite aggregates (Fig. 1). These clusters are similar to orthopyroxene–cordierite coronas around garnet, which are widespread in metapelites of the Bandelierkop Formation and are interpreted as produced by the reaction $Grt + Qtz = Opx + Crd$ at decompression and cooling of the metapelites (van Reenen et al., 2011 and references therein). In places, the orthopyroxene–cordierite clusters are recrystallized into equigranular aggregates of orthopyroxene, cordierite, plagioclase, and quartz with randomly scattered biotite flakes. Contacts between orthopyroxene and cordierite grains are lined by thin reaction structures: orthopyroxene–sillimanite and biotite–sillimanite–quartz symplectites. The cordierite and plagioclase grains are cut across by tiny veinlets of acicular sillimanite and quartz. These reaction textures were produced during subsobaric cooling of the granulite (van Reenen et al., 2011 and references therein).

Cylinders 4–6 mm long and 3.5–3.6 mm in diameter were prepared from sample PET-5 using a diamond drill. These cylinders were loaded into gold capsules 4 mm in diameter, 40 mm long, and with walls 0.2 mm thick. The free volume of the capsule with the sample was filled with mixtures of oxalic acid (which produced equimolar H_2O-CO_2 fluid with $X_{CO_2} = 0.5$) and KCl or NaCl. The concentrations of chlorides in the starting mixtures varied from 0.2 to 2.5 mol % (Table 2). The weights of the mixtures needed to fill the free volumes of the capsules in each experimental run were evaluated from the H_2O and CO_2 molar volumes under the experimental conditions, regardless of the volumes of the crystalline chlorides. The rock/fluid weight ratios in the experiments varied from 0.77 to 1.43 (Table 2). The capsules were welded using Lampert PUK 04 arc welder and a tungsten electrode in Ar atmosphere (to preclude significant capsule heating and fluid loss).

Although oxygen fugacity was not controlled in the experiments, we believe, based on estimates in our earlier experiments (Safonov et al., 2014a), that it was roughly equal to $\log f_{O_2} = NNO + 1$. Because the fluid was in excess with respect to the rock material, we did not expect any significant changes in the fluid composition (first of all, in the H_2O/CO_2 ratio) in the course of the experiments.

The experiments were carried out at a pressure of 600 MPa and temperature of 850°C in internal-heating gas-pressure apparatuses (gas bombs) at the Institute of Experimental Mineralogy (IEM), Russian Academy

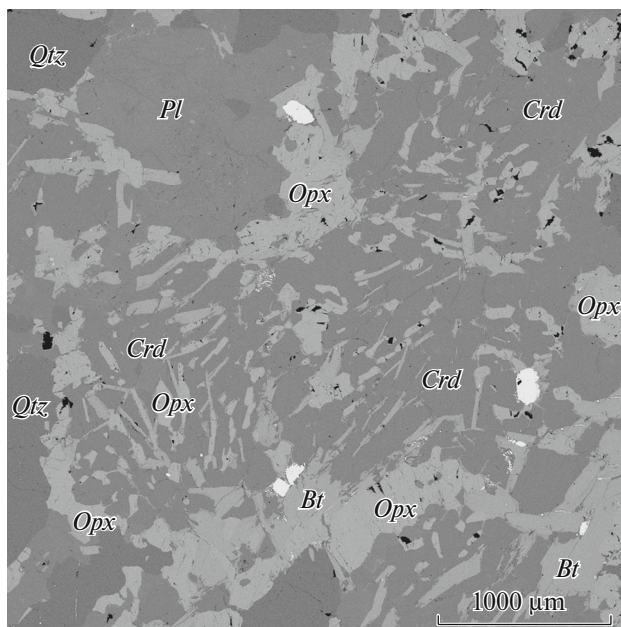


Fig. 1. BSE image of metapelite sample PET-5 (Safonov et al., 2014b) that was used in the experiments. Pale grains are aggregates of pyrrhotite, pentlandite, and chalcopyrite.

of Sciences. The experiments lasted for 10 days. Each capsule was weighed before and after experimental runs. Specific hissing of the opened capsules suggested that fluid in the capsules was preserved during isobaric quenching.

Analytical Techniques

After experiments, the capsules were placed into polyether mounts, cut parallel to the long axes, and polished using sand paper and diamond pastes. Before polishing, brittle samples were impregnated with epoxy resin in a vacuum impregnator.

The experimental products were analyzed on a CanScan MV2300 (VEGA TS 5130MM) and Tescan VEGA-II XMU scanning electron microscopes equipped with an INCA-Energy-350 EDS analytical setup and Oxford Inca Wave 700 WDS analytical setup. Crystalline phases were analyzed at 20 kV accelerating voltage and 10 nA current, with an electron beam 3 μm in diameter; the counting time was 100 s for all elements. The standards were quartz for Si and O, albite for Na, microcline for K, wollastonite for Ca, corundum for Al, metallic Mn, Fe, and Ti for these elements, respectively, periclase for MgO, halite for Cl, fluorite for F, and $LaPO_4$ for P.

The products of all experiments contained quenched melts (glasses), relics of minerals of the gneiss, and newly formed phases. To preclude Na loss, glasses were analyzed by scanning over areas of 20–180 μm². To eliminate the effects of diffusion halos in glass films in contact with crystalline phases (e.g.,

Table 1. Bulk composition of metapelite PET-5 and representative analyses of its major rock-forming minerals (Safonov et al., 2014b) used in the experiments

Component	Rock	<i>Crd</i>	<i>Bt</i>	<i>Opx</i>	<i>Pl</i>
SiO ₂	61.49	49.06	37.53	51.04	66.45
TiO ₂	0.70	0.07	5.66	0.19	0.00
Al ₂ O ₃	16.78	32.57	15.71	5.18	25.57
Cr ₂ O ₃	0.11	0.00	0.67	n.d.	0.00
FeO	8.28 [#]	4.55	13.47	23.64	0.22
MnO	0.07	0.00	0.00	0.28	0.00
MgO	7.43	9.89	13.69	19.73	0.11
CaO	1.52	0.12	0.07	0.16	5.88
Na ₂ O	2.09	0.18	0.01	0.08	8.87
K ₂ O	1.18	0.00	10.28	0.00	0.32
P ₂ O ₅	0.04	0.00	0.00	0.00	0.00
S	0.15	0.00	0.00	0.00	0.00
Total	99.84	96.44	95.07	100.30	107.42
Numbers of cations					
O		5	11	6	8
Si		5.057	2.733	1.900	2.744
Ti		0.005	0.310	0.005	0.000
Al		3.956	1.348	0.227	1.244
Cr		0.000	0.039	0.000	0.000
Fe		0.392	0.820	0.736	0.008
Mn		0.000	0.000	0.009	0.000
Mg		1.518	1.485	1.094	0.007
Ca		0.013	0.005	0.006	0.260
Na		0.036	0.001	0.006	0.710
K		0.000	0.955	0.000	0.017
P		0.000	0.000	0.000	0.000
S		0.000	0.000	0.000	0.000
X_{Mg}		0.790	0.640	0.595	
X_{Al}			0.201	0.057	
X_{Ca}					0.264

The bulk composition of the rock was analyzed by XRF on a PW2400 (Philips Analytical) spectrometer at the Institute of the Geology of Ore Deposits, Petrography, Mineralogy, and Geochemistry, Russian Academy of Sciences. [#] is Fe₂O₃.

Acosta-Vigil et al., 2006), the largest glass domains were analyzed. In each sample, glasses were analyzed at 10–30 spots in various parts of the glass domains. In spite of this, the compositions of the experimental glasses show notable variations (see below). Glasses in some of the samples were additionally analyzed on a Jeol JXA-8230 Superprobe at the Laboratory of Analytical Techniques of High Spatial Resolution at the Department of Petrology, Moscow State University, under analytical conditions recommended in (e.g., Acosta-Vigil et al., 2006) for analysis of hydrous granitic glasses: 20 kV accelerating voltage, 2 nA current, electron beam 20 μm in diameter, 40 s counting

time for Na and Al and 20 s for other elements. Comparison of analyses acquired using different techniques shows their good consistency.

PHASE ASSOCIATION IN THE EXPERIMENTAL PRODUCTS

Experiments with H₂O and Equimolar H₂O-CO₂ Fluids

Interaction between metapelite and H₂O fluid (experimental run MH6-18, Table 2) resulted in the most active melting of the rock. Cordierite and orthopyroxene were identified as relics among the melting

Table 2. Products and parameters of experiments on interaction of metapelite (sample PET-5) with H₂O, H₂O–CO₂, H₂O–CO₂–NaCl, and H₂O–CO₂–KCl fluids at 850°C and 600 MPa

Experimental run	m_g , g	m_{oa} , g	m_{ch} , g	$m_g/(m_{oa} + m_{ch})$	X_{salt}	a_{H_2O}	Experimental products
H ₂ O fluid							
MH6-18	0.1047	0.1073	0	0.9757	0	1	<i>Opx, Spl, Ilm, glass, Bt</i>
H ₂ O–CO ₂ fluid							
M6-19	0.1285	0.090	0	1.4277	0	0.608	<i>Opx, Spl, Ilm, glass</i>
H ₂ O–CO ₂ –NaCl fluid							
MN6-13	0.0526	0.0659	0.0003	0.7945	0.0026	0.599	1. <i>Amph + Opx + Ilm + glass</i> 2. <i>Na-Ged + Na-Bt + Spl + Ab + glass</i>
MN6-14	0.0547	0.0653	0.0009	0.8263	0.0075	0.582	1. <i>Opx + Ilm + glass</i> 2. <i>Opx + Na-Bt + Spl + Ilm + glass</i>
MN6-15	0.0568	0.0676	0.0017	0.8196	0.0131	0.563	1. <i>Opx + Ilm + Cpx + glass</i> 2. <i>Na-Ged + Na-Bt + Spl + Ab + glass</i>
MN6-16	0.0493	0.0610	0.0030	0.7703	0.0258	0.523	1. <i>Amph + Cpx + glass</i> 2. <i>Na-Bt + Spl + Ab + glass</i>
H ₂ O–CO ₂ –NaCl fluid							
MK6-10	0.0600	0.0669	0.0010	0.8836	0.0059	0.587	1. <i>Opx + Ilm + Bt + Pl + glass</i> 2. <i>Bt + Spl + Cor + glass</i>
MK6-11	0.0497	0.0602	0.0015	0.8055	0.0103	0.572	1. <i>Opx + Ilm + Bt + Pl + glass</i> 2. <i>Bt + Spl + Cor + glass</i>
MK6-12	0.0645	0.0624	0.0031	0.9847	0.0204	0.539	1. <i>Cpx + Ilm + Kfs + glass</i> 2. <i>Bt + Kfs + Cor + glass</i>

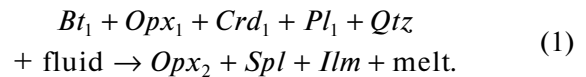
m_g is the weight of the rock cylinder, m_{oa} is the weight of oxalic acid, m_{ch} is the weight of the chloride, $m_g/(m_{oa} + m_{ch})$ is the starting rock/fluid weight ratio, X_{salt} is the mole fraction of the salt, NaCl/(NaCl + H₂O + CO₂) or KCl/(KCl + H₂O + CO₂), in the starting fluid, a_{H_2O} is the water activity in the starting fluid calculated for H₂O–CO₂–NaCl fluid by equation in (Aranovich et al., 2010). In all runs, a free fluid phase was present, as follows from the occurrence of round pores in the glasses. (1) Reaction products at contacts of biotite, orthopyroxene, plagioclase, and quartz in “tonalitic” domains of the metapelite, (2) products of cordierite replacement reactions or reactions at contacts of cordierite and orthopyroxene in “pelitic” domains of the rock.

products, whereas biotite, plagioclase, and quartz disappeared (Fig. 2a). Melting was associated with the origin of peritectic phases: spinel, newly formed orthopyroxene, and ilmenite. The newly formed orthopyroxene (*Opx*₂) occurs as small euhedral crystals in glass and rims around relics of the starting orthopyroxene (*Opx*₁, Fig. 2a). Numerous euhedral spinel crystals accompany *Opx*₂ (Fig. 2a), and ilmenite was found as inclusions in it. The occurrence of ilmenite inclusions in the orthopyroxene suggests that these phases were formed by the decomposition of the starting Ti-bearing biotite (Table 1). Although no relics of primary biotite were found in the sample, the glass contains thin biotite needles, which seem to be quench products of the water-saturated melt (Fig. 2a). Melt saturation with fluid also follows from the occurrence of round pores in the glass.

The products of interaction between the metapelite and equimolar H₂O–CO₂ fluid are analogous to the products of interaction between this rock and H₂O fluid (Fig. 2b). They are also newly formed orthopyroxene, ilmenite, and melt and differ only in a higher ilmenite content among the crystalline products of

interaction between metapelite and H₂O–CO₂ fluid (Fig. 2b). The degree of rock melting in the presence of H₂O–CO₂ fluid is also lower.

The interaction of the metapelite with H₂O and equimolar H₂O–CO₂ fluid can be schematically represented by the reaction



Experiments with H₂O–CO₂–NaCl Fluid

The products of experiments with H₂O–CO₂–NaCl fluid are of two types: (1) reaction products at contacts of biotite, plagioclase, and quartz in “tonalitic” domains of the metapelite and (2) products of replacement reactions of cordierite or reactions at contacts between cordierite and orthopyroxene in “pelitic” domains of the starting metapelite.

In run MN6-13 at a starting $X_{NaCl} = 0.0026$ in the fluid (Table 2), partial melting zones developed at contacts of primary biotite (*Bt*₁) with plagioclase and

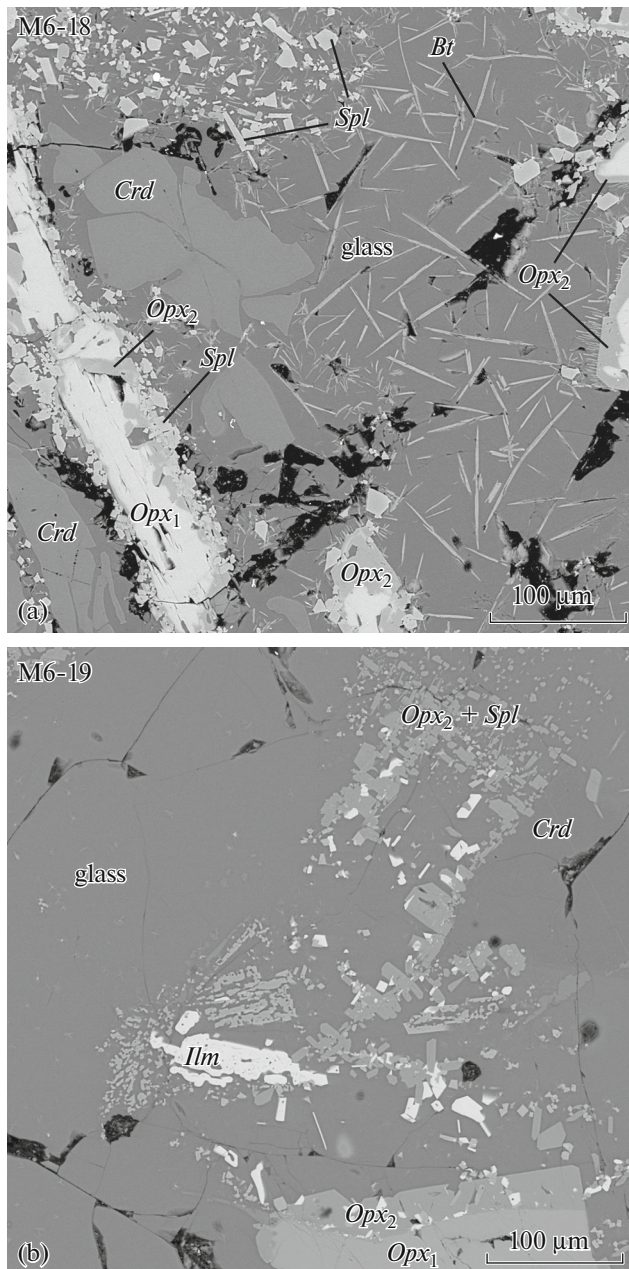
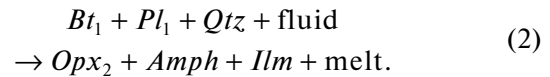


Fig. 2. Products of interaction between metapelite and (a) H_2O fluid and (b) equimolar H_2O-CO_2-NaCl fluid at $850^\circ C$ and 600 MPa.

quartz. These zones contain orthopyroxene (Opx_2), ilmenite, and Ca–Na amphibole (Fig. 3a), suggesting the peritectic reaction



In run MN6-15 at a starting $X_{NaCl} = 0.0131$ in the fluid (Table 2), this association is accompanied by small amounts of clinopyroxene. Clinopyroxene also appears along contacts of the starting orthopyroxene (Opx_1) with glass, while the orthopyroxene itself becomes more magnesian and less aluminous. No Ca–Na amphibole was found among the products of run MN6-15, but this mineral was identified among the products of run MN6-16 at $X_{NaCl} = 0.0258$ (Table 2). The mineral was found in association with clinopyroxene, Na-biotite (see below for its composition), and glass, which were formed along contacts of the starting biotite with orthopyroxene and plagioclase (Fig. 3b). The dominant newly formed phase among the products of run MN6-16 (Table 2) at $X_{NaCl} = 0.0258$ is Na-biotite. In “tonalitic” domains of the metapelite, it actively develops along boundaries of the starting orthopyroxene Opx_1 and biotite Bt_1 (Figs. 3c, 3d). The replacement of the starting biotite results in significantly zoned biotite flakes (Fig. 3d).

At the same NaCl concentrations in fluid, cordierite in the “pelitic” domains is replaced by an association of Na-bearing biotite, spinel, likely albite, and/or small amounts of melt (Fig. 3e). In the products of runs MN6-13, MN6-14, and MN6-15, the starting orthopyroxene (Opx_1) in contact with cordierite or products of its decomposition is replaced by an association of Na-bearing gedrite and spinel (Figs. 3e, 3f). In places, this association is accompanied by small amounts of newly formed orthopyroxene (Opx_2), which is richer in Al_2O_3 than the orthopyroxene in association with biotite decomposition products. The decomposition of cordierite or an association of cordierite with orthopyroxene in the presence of H_2O-CO_2-NaCl fluid can thus be represented by the schematic reaction

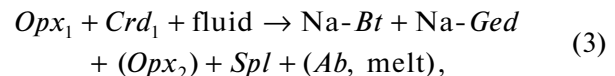
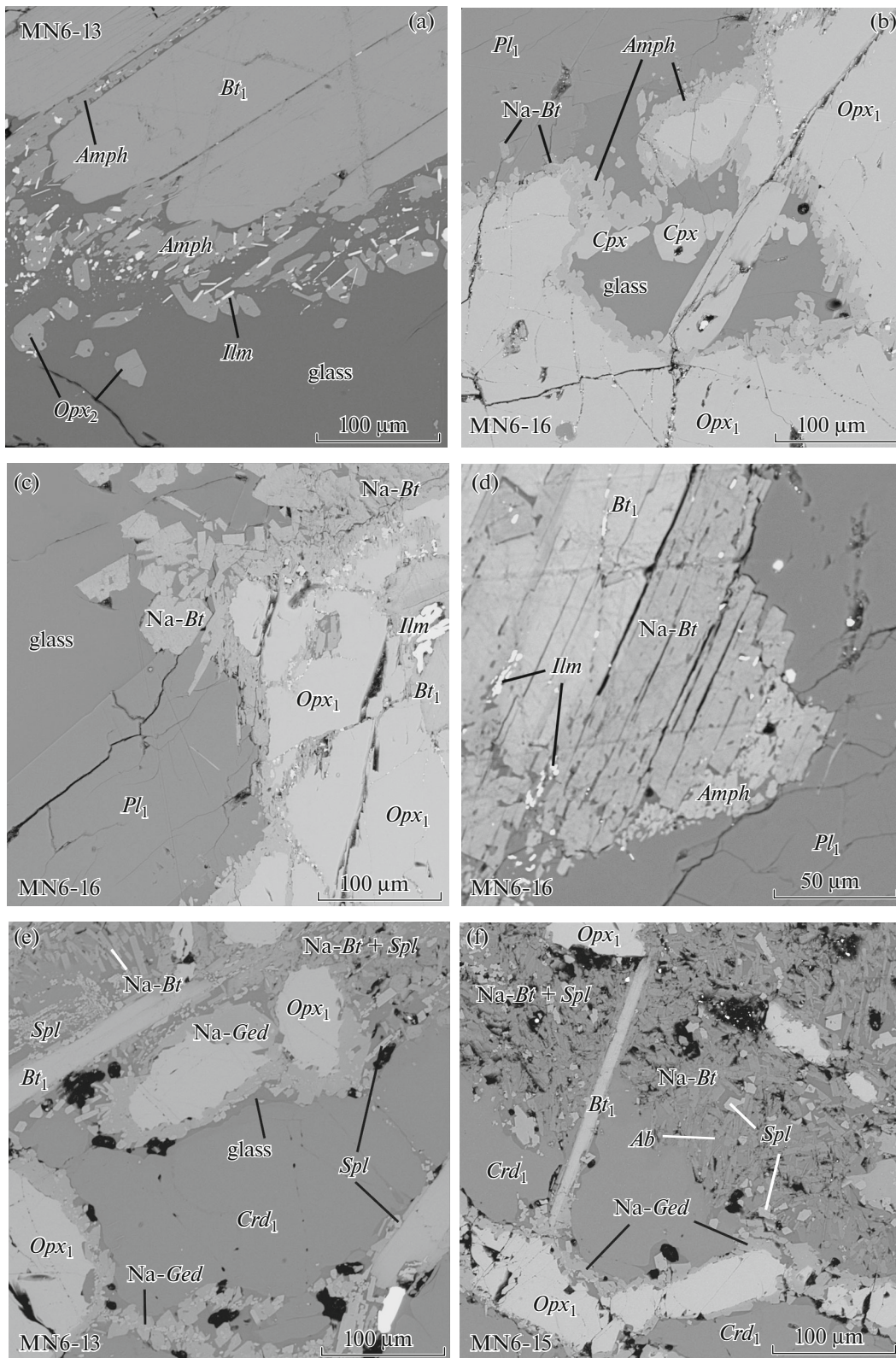


Fig. 3. Phase associations produced at interaction between metapelite and H_2O-CO_2-NaCl fluid at $850^\circ C$ and 600 MPa. (a) Incongruent biotite melting at contacts with plagioclase and quartz with the origin of pargasite amphibole and orthopyroxene. Run MN6-13, $X_{NaCl} = 0.0026$ (Table 2). (b) Association $Cpx + Ca-Na Amph + Na-Bt$ produced at the incongruent melting of the starting orthopyroxene (Opx_1) in the presence of starting plagioclase (Pl_1) in products of run MN6-16, $X_{NaCl} = 0.0258$ (Table 2). (c) Large flakes of Na-*Bt* replacing the starting orthopyroxene and biotite in the products of run MN6-16, $X_{NaCl} = 0.0258$ (Table 2). (d) Zoned biotite produced at the replacement of the starting biotite (Bt_1) by biotite richer in Na_2O ; in contact with plagioclase, biotite is replaced by a rim of Ca–Na amphibole. Run MN6-16, $X_{NaCl} = 0.0258$ (Table 2). (e) Reaction rims of Na-bearing gedrite (+ spinel) at contacts between the starting orthopyroxene (Opx_1) and cordierite (Crd_1). The starting biotite (Bt_1) is replaced by newly formed Na-bearing biotite. The reaction products are associated with minor amounts of melt (glass). Run MN6-13, $X_{NaCl} = 0.0026$ (Table 2). (f) Replacement of cordierite by the association Na-*Bt* + *Spl* + *Ab* (with a minor amount of melt) and reaction rims of Na-gedrite between cordierite and orthopyroxene in the products of run MN6-15, $X_{NaCl} = 0.0075$ (Table 2).



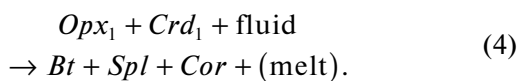
in which phases in parentheses occur in small volumes among the reaction products. No gedrite was identified among the products of run MN6-16, and Na-biotite is the dominant phase in the aggregates replacing cordierite.

Experiments with H₂O-CO₂-KCl Fluid

The products of experiments with H₂O-CO₂-KCl fluid also demonstrate reaction products of two types:

(1) associations formed by replacement of cordierite or cordierite in contact with orthopyroxene and (2) reaction products at contacts between biotite, plagioclase, and quartz.

In experimental products with H₂O-CO₂-KCl fluid at $X_{\text{KCl}} < 0.01$ in the starting fluid (experimental runs MK6-10 and MK-6-11, Table 2), the dominant newly formed phase is biotite (Figs. 4a–4d). It replaces the starting cordierite (Crd_1), orthopyroxene (Opx_1), and biotite (Bt_1). At contacts of cordierite and orthopyroxene with the starting biotite, newly formed biotite is usually found in association with rare spinel grains (Fig. 4a). When cordierite is replaced, elongate acicular corundum crystals are formed (Fig. 4b). All of these associations contain small amounts of glass. The decomposition of cordierite or its association with orthopyroxene in the presence of H₂O-CO₂-KCl fluid can be schematically represented by the reaction



Melting is obviously more intense in microassociations involving plagioclase and quartz (Fig. 4c). At contacts with quartz, the starting biotite incongruently melts with the formation of orthopyroxene poor in Al₂O₃ (see below) and ilmenite. In the presence of plagioclase, the starting biotite melts with the origin of orthopyroxene and ilmenite. At contacts with glass, the starting biotite is surrounded by zones of newly formed more magnesian biotite (Bt_2), which is poor in TiO₂. The starting orthopyroxene (Opx_1) is replaced by zones of newly formed orthopyroxene (Opx_2), which is more magnesian and much poorer in Al₂O₃ than the starting orthopyroxene. The starting plagioclase (Pl_1) decomposes to “spongy” zones of more calcic plagioclase (Pl_2) and glass (Fig. 4c). Such textures are widely known from experiments on plagioclase melting (e.g., Johannes, 1989; Acosta-Vigil et al., 2006).

In run MK6-12 at $X_{\text{KCl}} = 0.0204$ (Table 2), the foregoing associations additionally contain potassium feldspar. In the products of cordierite replacement, this phase occurs in equilibrium with newly formed biotite (Bt_2) and corundum (Fig. 4d). No spinel was found among the products of this experimental run. Plagioclase is intensely replaced in margins by potassium feldspar, and orthopyroxene and biotite in contact with it peritectically melt and produce minor amounts of clinopyroxene (Fig. 4e).

COMPOSITION OF CRYSTALLINE PHASES IN THE EXPERIMENTAL PRODUCTS

Pyroxenes

The composition of orthopyroxene in the products of metapelite interaction, sample PET-5, with H₂O, H₂O-CO₂, H₂O-CO₂-NaCl, and H₂O-CO₂-KCl fluids at 600 MPa and 850°C (Table 3) is notably different

from the composition of the starting orthopyroxene in this rock (Opx_1 in Fig. 5, $X_{\text{Mg}} = 0.60\text{--}0.66$, $X_{\text{Al}} = 0.04\text{--}0.06$). Orthopyroxene in the products of runs with H₂O and H₂O-CO₂ fluids is the richest in Al (Table 3). The orthopyroxene of run M6-19 (H₂O-CO₂ fluid) has $X_{\text{Al}} = 0.09\text{--}0.11$ at $X_{\text{Mg}} = 0.66\text{--}0.73$ (Fig. 5, Table 3). Interaction with H₂O fluid (run MN-18) produces more magnesian orthopyroxene with $X_{\text{Al}} = 0.07\text{--}0.09$ (Fig. 5, Table 3).

An indicator difference of orthopyroxene in the products of runs on interaction of the metapelite with NaCl- or KCl-bearing fluids from this phase in products of runs with H₂O and H₂O-CO₂ fluids is low X_{Al} values (Fig. 5, Table 3), which is lower than in the starting orthopyroxene. The lowest X_{Al} values were found in orthopyroxene from the products of run MN6-15, in which the NaCl concentration was at a maximum (Fig. 5, Table 3). All of the low aluminous orthopyroxenes were produced by incongruent melting of the starting biotite or by interaction of the starting orthopyroxene and generated melts. However, the cordierite decomposition products in samples MN6-14 and MN6-15 contain individual tiny orthopyroxene crystals with elevated X_{Al} (Fig. 5, fields contoured with dashed lines). These crystals are usually constrained to small pools of peraluminous melt in decomposition products of cordierite. We cannot rule out that these orthopyroxene crystals may be quench products of the melt.

Clinopyroxene was identified in the products of runs MN6-15, MN6-16, and MK6-12 (Table 2, Figs. 3b, 4e), in which this mineral was produced by incongruent melting reactions of biotite and/or orthopyroxene with plagioclase in the presence of H₂O-CO₂-salt fluid. In runs MN6-15 and MK6-12, clinopyroxene has similar magnesian number ($X_{\text{Mg}} = 0.71\text{--}0.75$); in run MN6-16, its $X_{\text{Mg}} = 0.47\text{--}0.48$ (Table 3). In the formulas of the clinopyroxene, Na/Al > 1, with clinopyroxene in run MN6-16 has Na/Al = 12–15 (Table 3). This indicates that the clinopyroxene is rich in the aegirine end member.

Micas

The decomposition products of cordierite in the presence of H₂O-CO₂-NaCl fluid contain micas with broadly varying Na/(Na + K) ratios (Figs. 6a, 6b, Table 4). This points out that the mica solid solution contains variable concentrations of the aspidolite end member NaMg₃AlSi₃O₁₀(OH)₂. The Na/(Na + K) ratio of micas is a function of NaCl concentration in the starting fluid, and micas with the highest ratios Na/(Na + K) = 0.83–0.90, which correspond to 5.7–6.1 wt % Na₂O, were synthesized in run MN6-16 at the maximum NaCl concentration in the fluid (Fig. 6b, Table 4). An increase in the Na/(Na + K) ratio is associated with a small decrease in the Si concentra-

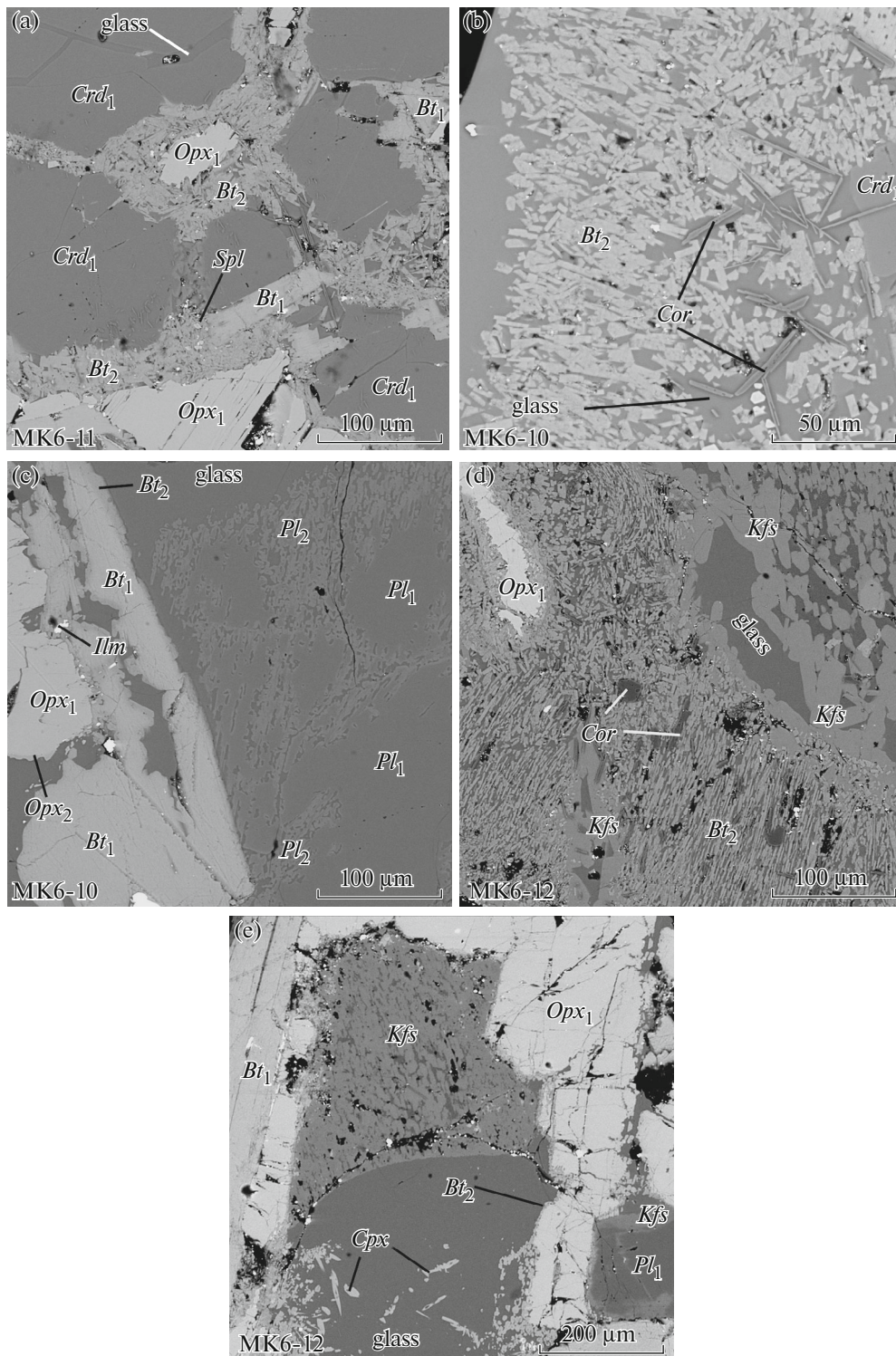


Fig. 4. Phase associations produced at interaction between metapelite and $\text{H}_2\text{O-CO}_2\text{-KCl}$ fluids at 850°C and 600 MPa. (a) Reaction rims of biotite at contacts between the starting orthopyroxene (Opx_1), cordierite (Crd_1), and biotite (Bt_1). The rims are associated with spinel and minor amounts of melt. Run MK6-11, $X_{\text{KCl}} = 0.0103$ (Table 2). (b) Replacement of cordierite (Crd_1) by an association of biotite (Bt_2), corundum, and glass. Run MK6-10, $X_{\text{KCl}} = 0.0059$ (Table 2). (c) Melting of the starting plagioclase (Pl_1) in association with biotite (Bt_1) and orthopyroxene (Opx_1). More calcic plagioclase (Pl_2) forms “spongy” textures with glass around relics of the starting plagioclase. The biotite and orthopyroxene develop outer zones of higher X_{Mg} (Bt_2 and Opx_2). Bt_1 contains 5.6 wt % TiO_2 , whereas Bt_2 contains 2.1 wt % TiO_2 . Opx_1 contains 5.1 wt % Al_2O_3 , and Opx_2 contains 1.6 wt % Al_2O_3 . (d) Potassium feldspar among the decomposition products of cordierite. Run MK6-12, $X_{\text{KCl}} = 0.0204$ (Table 2). (e) Association of clinopyroxene and potassium feldspar among the products of incongruent melting of the starting association of biotite and orthopyroxene in run MK6-12, $X_{\text{KCl}} = 0.0204$ (Table 2). The starting plagioclase is actively replaced by potassium feldspar.

Table 3. Representative analyses of pyroxenes in the run products

Component	MH6-18		M6-19		MN6-13			MN6-14			MN6-15				MN6-16		MK6-10		MK6-12		
	1	2	2	1	3	3	3	4	1	2	2	2	1	2	5	2	2	1	1	6	
SiO ₂	52.82	51.33	48.62	49.17	54.73	55.62	53.88	47.97	53.86	52.63	53.03	55.18	54.90	54.42	53.94	54.04	53.98	55.63	54.42	53.23	52.10
TiO ₂	0.25	0.27	0.44	0.42	0.16	0.07	0.58	1.87	0.05	0.15	0.36	0.14	0.12	0.17	0.19	0.00	0.17	0.20	0.06	0.05	0.00
Al ₂ O ₃	6.76	7.84	8.03	8.44	8.28	1.29	2.45	8.30	2.45	2.47	2.97	0.43	0.57	0.66	0.81	1.31	0.58	0.12	1.49	1.58	0.22
FeO	12.00	10.99	12.66	15.80	17.77	18.33	15.88	20.76	16.13	17.75	17.46	15.71	16.56	18.08	8.64	9.28	17.74	16.13	17.27	18.83	8.74
MnO	0.10	0.17	0.04	0.06	0.30	0.28	0.00	0.04	0.21	0.07	0.05	0.59	0.29	0.10	0.05	0.25	0.13	0.58	0.41	0.24	0.12
MgO	28.51	27.81	27.54	24.55	23.02	25.53	26.97	20.93	26.40	25.10	24.96	27.47	26.47	24.83	13.32	13.69	8.67	26.21	26.16	23.46	12.89
CaO	0.12	0.02	0.07	0.35	0.27	0.73	0.88	0.10	0.69	0.58	0.37	0.07	0.34	0.84	22.29	21.59	14.03	0.88	0.49	0.57	23.84
Na ₂ O	0.05	0.04	0.18	0.00	0.20	0.24	0.00	0.09	0.39	0.33	0.08	0.05	0.18	0.18	1.09	0.63	5.14	0.24	0.00	0.19	0.58
Cr ₂ O ₃	0.00	0.18	0.29	0.57	0.45	0.60	0.09	0.74	0.65	0.19	0.16	0.07	0.04	0.32	0.12	0.44	0.12	0.53	0.09	0.25	0.06
Total	100.61	98.65	100.75	99.01	99.02	101.89	100.70	100.71	100.83	99.27	99.44	99.71	99.47	99.60	100.45	101.23	100.56	100.52	100.39	98.40	99.49

Component	Numbers of cations per 6 oxygen atoms																							
	1	2	3	4	5	6	1	2	3	4	5	6	1	2	3	4	5	6	1	2	3	4	5	6
Si	1.855	1.831	1.816	1.779	1.809	1.798	1.963	1.987	1.935	1.766	1.934	1.936	1.993	1.995	1.992	2.001	1.989	2.060	2.039	2.004	1.968	1.980	1.980	1.987
Ti	0.007	0.007	0.012	0.017	0.012	0.014	0.004	0.002	0.016	0.052	0.001	0.010	0.004	0.003	0.005	0.005	0.000	0.005	0.007	0.005	0.002	0.001	0.007	0.000
Al	0.280	0.330	0.334	0.364	0.371	0.360	0.055	0.050	0.104	0.360	0.104	0.128	0.018	0.024	0.028	0.035	0.057	0.026	0.021	0.005	0.063	0.069	0.032	0.010
Fe	0.352	0.328	0.373	0.483	0.546	0.526	0.550	0.474	0.527	0.639	0.484	0.533	0.474	0.503	0.553	0.268	0.286	0.566	0.554	0.486	0.522	0.585	0.246	0.279
Mn	0.003	0.005	0.001	0.002	0.002	0.009	0.009	0.000	0.000	0.001	0.006	0.002	0.018	0.009	0.003	0.002	0.008	0.004	0.004	0.018	0.013	0.008	0.000	0.004
Mg	1.491	1.478	1.446	1.338	1.223	1.267	1.364	1.435	1.355	1.148	1.413	1.358	1.478	1.433	1.354	0.736	0.751	0.493	0.519	1.406	1.409	1.300	0.729	0.732
Ca	0.005	0.001	0.003	0.014	0.001	0.011	0.028	0.034	0.030	0.004	0.027	0.014	0.003	0.013	0.033	0.885	0.851	0.573	0.633	0.034	0.019	0.023	0.976	0.973
Na	0.003	0.003	0.012	0.000	0.014	0.000	0.017	0.000	0.000	0.006	0.027	0.006	0.004	0.013	0.013	0.078	0.045	0.380	0.320	0.017	0.000	0.014	0.055	0.043
Cr	0.000	0.005	0.008	0.016	0.015	0.013	0.017	0.003	0.021	0.019	0.018	0.005	0.002	0.001	0.009	0.004	0.013	0.004	0.004	0.015	0.003	0.007	0.000	0.002
X _{Mg}	0.81	0.82	0.79	0.73	0.69	0.71	0.71	0.75	0.72	0.64	0.74	0.72	0.76	0.74	0.71	0.73	0.72	0.47	0.48	0.74	0.73	0.69	0.75	0.72
X _{Al}	0.07	0.08	0.08	0.09	0.09	0.09	0.01	0.01	0.03	0.09	0.03	0.03	0.00	0.01	0.01					0.00	0.02	0.02		

(1) Outer zones on the starting orthopyroxene (Table 1), (2) euhedral crystals in glass, (3) in association with Ca-Na amphibole (Fig. 4a), (4) small crystals among the cordierite replacement products, (5) crystals in glass in contact with the starting orthopyroxene, (6) in association with potassium feldspar.

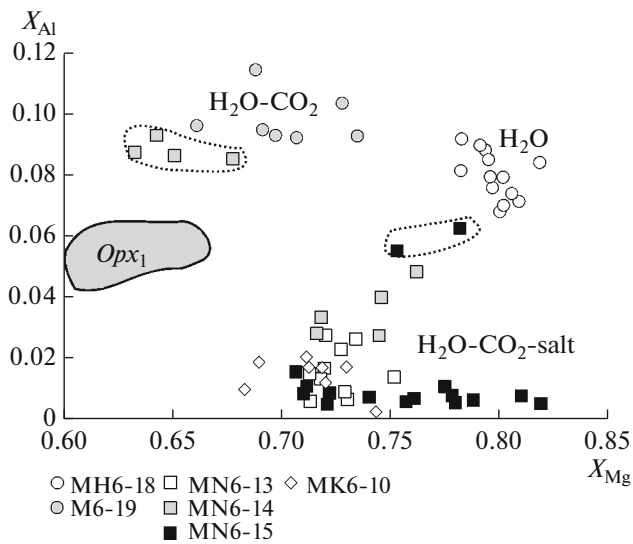


Fig. 5. Variations of X_{Mg} and X_{Al} of orthopyroxene in the products of experiments on interaction of metapelite with H_2O , H_2O-CO_2 , H_2O-CO_2-NaCl , and H_2O-CO_2-KCl fluids at 600 MPa and 850°C. The field of Opx_1 shows the variations in the orthopyroxene composition in starting metapelite sample PET-5 (Safonov et al., 2014b). Dashed lines contour the composition fields of single small orthopyroxene crystals in association with decomposition products of cordierite in runs MN6-14 (pale gray squares) and MN6-15 (dark gray squares).

tion and an increase in that of Al, i.e., with shift of the compositions toward the preiswerkite (Na-eastonite) component $NaMg_2Al_3Si_2O_{10}(OH)_2$ (e.g., Visser et al., 1999). Micas synthesized in the runs with H_2O-CO_2-KCl fluids also show elevated $Na/(Na + K)$ ratios, up to 0.09–0.11 (i.e., contain up to 0.7–0.9 wt % Na_2O) in the micas of run MK6-10 (Table 4). These concentrations are comparable with the maximum Na_2O concentrations ever found in biotite from granulite-facies metapelites (Grew et al., 1987). An increase in the KCl concentration in the fluid leads to a decrease in this ratio, although it remains higher than in the starting biotite in metapelite sample PET-5 (Bt_1 in Fig. 6a).

Micas in the experimental products are usually more magnesian than the starting biotite in sample PET-5, $X_{Mg} = 0.62–0.65$ (Table 4). The most magnesian micas ($X_{Mg} = 0.83–0.84$) were found among the decomposition products of cordierite in run MN6-16. The Mg mole fraction of the mica replacing orthopyroxene and starting biotite is notably lower: $X_{Mg} = 0.68–0.70$. Analogous relations between biotite compositions were observed in other runs carried out with H_2O-CO_2-NaCl fluid. The X_{Mg} of biotite replacing cordierite in experiments with H_2O-CO_2-KCl fluid is similar and varies within the range $X_{Mg} = 0.65–0.73$, i.e., is close to this parameter of the starting biotite.

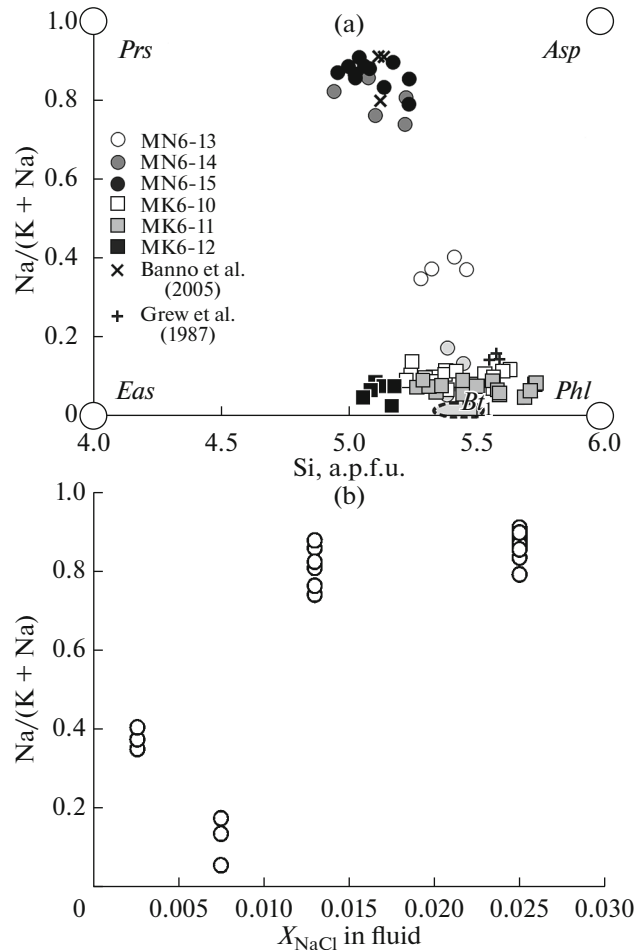


Fig. 6. Composition of micas and run products. (a) Variations in the proportions of end members of the mica solid solution. *Eas*—eastonite, *Prs*—preiswerkite, *Asp*—aspidolite, *Phl*—phlogopite. Times sign—composition of natural aspidolite (Banno et al., 2005), cross—composition of Na-bearing phlogopite in metapelites from western Greenland (Grew et al., 1987). The gray field of Bt_1 contoured with a dashed line shows the composition of the starting biotite in metapelite sample PET-5. (b) Dependence of the $Na/(K + Na)$ ratio of the micas on the NaCl concentration of the starting fluid.

In contrast to the starting biotite in sample PET-5, which contains 4.5–6 wt % TiO_2 (Table 1), the newly formed biotite commonly contains less than 0.3 wt % TiO_2 (Table 4). Biotite with low TiO_2 concentrations is typical of the decomposition products of cordierite (Figs. 3b, 3c, 4b, 4d) or reaction rims between cordierite and orthopyroxene (Fig. 4a). TiO_2 concentrations greater than 1 wt %, and reaching 3–4 wt %, are typical of the significantly modified zoned relics of the starting biotite (Figs. 3c, 3d, 4c, Bt_1) and newly formed biotite flakes replacing them (Table 4). This biotite is usually accompanied by newly formed ilmenite.

The biotite produced at interaction between the metapelite and chloride-bearing fluid is characterized

Table 4. Representative analyses of micas in the run products

Component	MN6-13		MN6-14		MN6-15		MN6-16			MK6-10			MK6-11		MK6-12		
	1	1	3	3	1	1	2	2	3	1	1	3	4	1	5	5	
SiO ₂	38.76	38.92	37.67	37.21	37.15	38.04	35.34	36.01	37.99	36.81	35.12	37.61	36.59	37.67	35.29	35.22	
TiO ₂	0.00	0.49	3.88	4.13	0.00	0.00	0.96	1.72	3.35	0.05	0.01	1.37	0.01	0.32	0.00	0.05	
Al ₂ O ₃	22.08	19.85	16.94	17.19	22.92	23.21	22.85	20.04	15.51	20.93	21.83	16.65	18.83	16.13	24.42	24.26	
FeO	7.62	8.14	12.19	11.37	7.75	9.74	11.87	12.40	14.51	10.56	10.31	11.04	12.49	10.98	10.62	9.23	
MnO	0.00	0.00	0.19	0.02	0.10	0.07	0.06	0.00	0.00	0.05	0.04	0.04	0.16	0.24	0.06	0.14	
MgO	20.04	19.85	15.56	15.77	18.91	18.59	16.13	16.12	15.22	15.75	15.57	16.88	16.19	16.57	14.90	14.17	
CaO	0.04	0.18	0.00	0.06	0.00	0.01	0.00	0.00	0.10	0.15	0.08	0.00	0.00	0.16	0.06	0.05	
Na ₂ O	2.53	2.60	0.89	1.24	5.41	5.77	6.67	5.56	3.89	0.69	0.73	0.70	0.37	0.43	0.66	0.59	
K ₂ O	6.41	6.51	8.69	8.90	2.90	2.09	1.02	2.24	3.68	9.61	9.40	9.50	9.34	9.13	10.37	10.55	
Cr ₂ O ₃	0.14	0.00	0.49	0.47	0.00	0.13	0.10	0.00	0.67	0.05	0.00	0.77	0.38	0.35	0.01	0.00	
Cl	0.01	0.05	0.06	0.05	0.00	0.05	0.00	0.05	0.02	0.12	0.03	0.05	0.19	0.14	0.08	0.00	
Total	97.63	96.59	96.56	96.41	95.14	97.70	95.00	94.14	94.94	94.77	93.12	94.61	94.55	92.12	96.47	94.26	
Numbers of cations per 22 oxygen atoms																	
Si	5.322	5.457	5.445	5.384	5.218	5.222	5.039	5.232	5.562	5.398	5.239	5.562	5.441	5.707	5.101	5.176	
Ti	0.000	0.052	0.422	0.449	0.000	0.000	0.103	0.188	0.369	0.006	0.001	0.152	0.001	0.036	0.000	0.006	
Al	3.572	3.280	2.886	2.931	3.793	3.754	3.839	3.431	2.676	3.616	3.837	2.901	3.300	2.879	4.160	4.201	
Fe	0.875	0.954	1.473	1.375	0.910	1.118	1.415	1.506	1.776	1.294	1.286	1.365	1.553	1.390	1.283	1.134	
Mn	0.000	0.000	0.023	0.002	0.012	0.008	0.007	0.000	0.000	0.006	0.005	0.005	0.020	0.031	0.007	0.017	
Mg	4.098	4.146	3.351	3.399	3.956	3.801	3.426	3.489	3.320	3.440	3.460	3.718	3.586	3.739	3.208	3.102	
Ca	0.006	0.027	0.000	0.009	0.000	0.001	0.000	0.000	0.016	0.024	0.013	0.000	0.000	0.026	0.009	0.008	
Na	0.673	0.706	0.249	0.348	1.472	1.535	1.843	1.565	1.104	0.196	0.211	0.201	0.107	0.126	0.185	0.168	
K	1.122	1.164	1.602	1.642	0.519	0.366	0.185	0.415	0.687	1.797	1.788	1.792	1.771	1.764	1.912	1.977	
Cr	0.015	0.000	0.056	0.054	0.000	0.014	0.011	0.000	0.077	0.006	0.000	0.090	0.045	0.042	0.001	0.000	
Cl	0.002	0.000	0.015	0.012	0.000	0.012	0.000	0.012	0.005	0.030	0.008	0.013	0.048	0.036	0.020	0.000	
X _{Mg}	0.82	0.81	0.69	0.71	0.81	0.77	0.71	0.70	0.65	0.73	0.73	0.73	0.70	0.72	0.71	0.73	
X _{Al}	0.26	0.24	0.21	0.22	0.27	0.27	0.28	0.25	0.20	0.26	0.28	0.21	0.24	0.21	0.30	0.31	
X _{Na}	0.37	0.37	0.13	0.17	0.74	0.81	0.91	0.79	0.61	0.10	0.10	0.10	0.06	0.07	0.09	0.08	

(1) Among cordierite replacement products, (2) large flakes in glass (Fig. 4d), (3) outer zones of the starting biotite (for example, Bt_2 in Figs. 4d, 5c), (4) reaction rim between cordierite and orthopyroxene (Fig. 5a), (5) in association with potassium feldspar and corundum (Fig. 5d).

by low Cl concentrations (Table 4). For example, the Na-bearing micas from experiments with H₂O-CO₂-NaCl fluid usually contains no more than 0.05 wt % Cl. Such low Cl concentrations are explained first of all by the high X_{Mg} of this biotite. At the same time, we cannot rule out that an additional factor unfavorable for Cl accommodation in biotite is elevated Na concentration (because Na is a smaller cation than K). Indeed, biotite of similar X_{Mg} in experiments with H₂O-CO₂-KCl fluid contains higher Cl concentrations, up to 0.10–0.15 wt %.

Amphiboles

Gedrite is formed at interaction of cordierite and orthopyroxene in the presence of H₂O-CO₂-NaCl fluid (runs MN6-13 and MN6-15; Table 2, Figs. 3b, 3c). The gedrite is characterized by a high Na₂O concentration (Table 5), which exceeds 3.5 wt % in some analyses of gedrite from run MN6-15. The great majority of the analyzed gedrite grains show a linear negative correlation between (Na + Al) and Si in formulas normalized to 23 oxygen ions (Fig. 7a), as is typical of isomorphism ${}^{\text{A}}\square + {}^{\text{T}}\text{Si} \leftrightarrow {}^{\text{A}}\text{Na} + {}^{\text{T}}\text{Al}$ (where ${}^{\text{A}}\square$ is a vacancy at site A) in orthorhombic amphiboles (Hawthorn et al., 2008). However, the composition points of the gedrite with >3.5 wt % Na₂O plot away from this trend. In the Na–Al^[6] diagram (Fig. 7b), the composition points of this gedrite cluster near the end member of the solid solution NaMg₂(Mg₃Al₂)(Si₅Al₃)O₂₂(OH)₂ (Hawthorne et al., 2008). The maximum measured Na₂O concentration in gedrite from the products of run MN6-15 is 3.91 wt %. This is notably higher than the highest Na₂O concentration ever analyzed in gedrite from granulite-facies rocks (3.06 wt %; Tsunogae et al., 2007). Comparison of the compositions of gedrite from runs MN6-13 and MN6-15, which were conducted with different X_{NaCl} in the fluid (Table 2), shows that Na₂O concentration in gedrite is a function of NaCl concentration in the starting fluid. The Cl concentration of the gedrite does not exceed 0.1 wt % (Table 5).

The composition of Ca-Na amphibole found among the products of incongruent melting of biotite in the presence of plagioclase and quartz in run MN6-13 (Fig. 3a) corresponds to the pargasite–edenite series (Table 5). The proportions of the pargasite and edenite components in amphibole from run MN6-13 are roughly 50/50, whereas the composition of amphibole in run MN6-15 is shifted toward edenite. Continuing this tendency, the composition of Ca-Na amphibole replacing orthopyroxene in run MN6-16 (Fig. 3b) is shifted toward winchite. The Ca-Na amphibole is typically rich in TiO₂ (2–3 wt %), which is explained by the production of this mineral after the starting Ti-bearing biotite (Table 5).

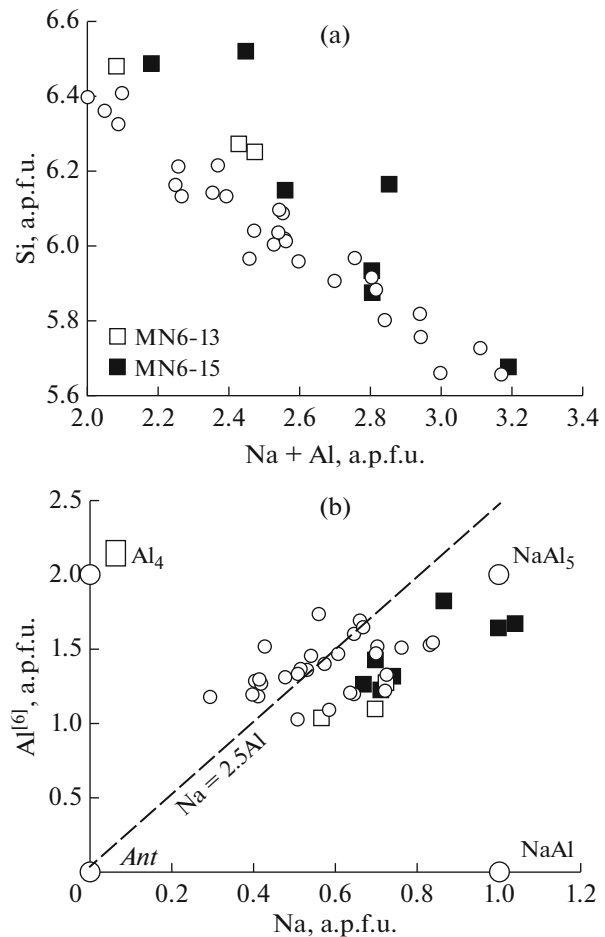


Fig. 7. Composition of gedrite in the products of runs MN6-13 and MN6-15 (Table 2). (a) Negative correlation between the total (Na + Al) and Si concentrations in the gedrite formulae. (b) Proportions of octahedrally coordinated Na and Al in the gedrite formulae. End members of the orthorhombic amphibole solid solution (Hawthorne et al., 2008): *Ant*—anthophyllite Mg₂Mg₅Si₈O₂₂(OH)₂, $\square\text{Al}_4$ — $\square\text{Mg}_2(\text{Mg}_3\text{Al}_2)(\text{Si}_6\text{Al}_2)\text{O}_{22}(\text{OH})_2$, NaAl₅—NaMg₂(Mg₃Al₂)(Si₆Al₃)O₂₂(OH)₂, NaAl—NaMg₂Mg₆(Si₇Al)O₂₂(OH)₂. The dashed line corresponds to Na = 2.5Al, which was derived for orthorhombic amphiboles from the charge balance condition (Hawthorne et al., 2008). Circles show the composition of Na-bearing gedrite in granulite-facies metapelites (Dasgupta et al., 1999; Tsunogae et al., 2007; Kanazawa et al., 2009; Safonov et al., 2014a).

Spinel

The spinel is a product of incongruent melting of cordierite in the experiments with H₂O and H₂O-CO₂ fluids (Figs. 2a, 2b). The spinel formed in equilibrium with H₂O fluid (run MN6-19) has $X_{\text{Mg}} = 0.63$ – 0.65 , while the spinel synthesized in equilibrium with H₂O-CO₂ fluid is richer in Fe and has $X_{\text{Mg}} = 0.44$ – 0.46 . These differences are likely explained by the more active melting of cordierite in the presence of H₂O fluid.

Table 5. Representative analyses of amphiboles in the run products

Component	MN6-13				MN6-15				MN6-16	
	1	1	2	2	1	1	2	2	3	3
SiO ₂	45.85	46.20	47.42	45.91	46.10	44.30	48.16	43.88	48.61	49.01
TiO ₂	2.38	3.03	0.13	0.00	2.99	5.12	0.31	0.26	0.35	0.33
Al ₂ O ₃	11.54	11.80	15.92	18.88	8.29	8.61	19.61	18.64	5.89	6.78
FeO	10.99	10.00	12.03	11.42	9.99	12.20	14.17	11.71	13.17	13.68
MnO	0.00	0.64	0.03	0.42	0.30	0.00	0.00	0.13	0.07	0.17
MgO	16.47	14.90	21.94	20.64	15.40	14.40	14.91	20.50	15.14	16.76
CaO	8.97	10.40	0.35	0.18	10.00	9.76	0.70	0.05	8.57	7.71
Na ₂ O	2.35	2.53	2.12	2.74	2.69	2.45	3.68	2.62	4.17	3.41
K ₂ O	0.20	0.32	0.02	0.00	0.20	0.19	0.18	0.00	0.31	0.31
Cr ₂ O ₃	0.89	0.64	0.04	0.30	1.05	0.82	0.05	0.01	0.12	0.34
Cl	0.00	0.00	0.10	0.08	0.00	0.00	0.00	0.11	0.00	0.00
Total	99.64	100.46	100.10	100.57	97.01	97.85	101.77	97.91	96.40	98.50
Numbers of cations per 23 oxygen atoms										
Si	6.534	6.532	6.476	6.247	6.778	6.531	6.516	6.149	7.204	7.098
Ti	0.255	0.322	0.013	0.000	0.331	0.567	0.032	0.027	0.039	0.036
Al	1.938	1.963	2.562	3.027	1.437	1.495	3.126	3.078	1.029	1.157
Fe	1.309	1.186	1.373	1.299	1.228	1.503	1.603	1.372	1.632	1.656
Mn	0.000	0.077	0.003	0.048	0.037	0.000	0.000	0.015	0.009	0.021
Mg	3.496	3.139	4.463	4.183	3.380	3.152	3.005	4.279	3.342	3.616
Ca	1.369	1.569	0.051	0.026	1.580	1.540	0.101	0.008	1.360	1.196
Na	0.649	0.693	0.561	0.722	0.767	0.700	0.965	0.711	1.198	0.957
K	0.036	0.058	0.003	0.000	0.038	0.036	0.031	0.000	0.059	0.057
Cr	0.100	0.072	0.004	0.032	0.122	0.095	0.005	0.001	0.014	0.039
Cl	0.000	0.000	0.023	0.018	0.000	0.000	0.000	0.026	0.000	0.000

(1) In association with orthopyroxene in partial melting zones of biotite, plagioclase, and quartz (Fig. 4a), (2) reaction rims between cordierite and orthopyroxene (Figs. 4e, 4f), (3) rims around orthopyroxene (Fig. 4b).

Spinel was found among the cordierite decomposition products in all runs with H₂O-CO₂-salt fluids (Figs. 3b, 3c, 4a). Nevertheless, in the runs with H₂O-CO₂-KCl fluid, spinel is a notably rarer phase, and a typical aluminous phase among the cordierite decomposition products is corundum (Figs. 4b, 4d). The Mg mole fraction of spinel in the runs with H₂O-CO₂-NaCl fluids varies from 0.52 to 0.69. The most magnesian spinel ($X_{Mg} = 0.62-0.69$) is typical of the products of run MN6-16, which was conducted with a maximum NaCl concentration in the fluid. Conversely, the rare spinel in the products of runs with H₂O-CO₂-KCl fluids has a notably lower $X_{Mg} = 0.40-0.49$.

The spinel is commonly relatively poor in Cr₂O₃, whose concentration is higher than 1 wt % only in rare analyses. The occurrence of Cr in the spinel among the decomposition products of cordierite is likely explained by that the reaction involves the starting orthopyroxene and/or biotite, which are relatively rich in Cr in the metapelite of sample PET-5 (Safonov

et al., 2014b). The newly formed spinel typically contains a ZnO admixture.

Feldspars

Albite identified among the decomposition products of cordierite in the presence of H₂O-CO₂-NaCl fluid usually contains 0.3–0.6 wt % K₂O and up to 1–2 wt % CaO.

No significant changes in the composition of the starting plagioclase were detected in melting reactions in the presence of H₂O-CO₂-NaCl reactions. Plagioclase melting in run MK6-10 (with the development of “spongy” zones with glass inclusions, Fig. 4c) results in a significant increase in the X_{Ca} of the plagioclase, from 0.30–0.31 typical of the starting plagioclase in sample PET-5 to 0.50–0.53. This remarkable plagioclase zoning induced by melting is explained by the slow diffusion of components in pla-

Table 6. Average compositions (normalized to 100 wt %) of melts pooling among run products

Component	MH6-18	M6-19	MN6-13	MN6-14	MN6-15	MN6-16	MK6-10	MK6-11	MK6-12
	16*	11	17	8	20	14	22	9	12
SiO ₂	70.96(1.08)	69.15(0.45)	74.55(1.18)	73.47(1.15)	75.07(0.54)	62.94(0.76)	73.51(1.90)	72.71(1.91)	74.57(1.01)
TiO ₂	0.77(0.13)	0.60(0.1)	0.45(0.21)	0.24(0.10)	0.17(0.06)	0.29(0.12)	0.23(0.16)	0.13(0.11)	0.26(0.11)
Al ₂ O ₃	18.44(0.47)	17.01(0.13)	14.13(0.62)	14.95(0.72)	13.88(0.37)	20.52(0.62)	14.42(1.33)	14.92(1.39)	11.88(0.75)
FeO	2.13(0.33)	2.33(0.21)	1.24(0.18)	1.34(0.13)	1.20(0.13)	2.01(0.21)	1.51(0.21)	1.11(0.16)	1.74(0.21)
MnO	0.09(0.05)	0.06(0.05)	0.03(0.03)	0.05(0.05)	0.06(0.08)	0.05(0.05)	0.07(0.08)	0.05(0.06)	0.10(0.07)
MgO	1.26(0.19)	1.04(0.29)	0.45(0.18)	0.64(0.06)	0.40(0.07)	0.45(0.11)	0.56(0.13)	0.44(0.10)	0.19(0.05)
CaO	2.60(0.14)	2.43(0.13)	1.51(0.16)	1.89(0.17)	1.16(0.14)	0.61(0.13)	1.68(0.31)	1.70(0.15)	0.30(0.10)
Na ₂ O	1.87(0.51)	3.80(0.23)	5.18(0.20)	4.21(0.20)	5.99(0.21)	10.34(0.38)	3.25(0.23)	3.15(0.31)	3.13(0.26)
K ₂ O	1.42(0.13)	3.23(0.19)	2.05(0.16)	2.70(0.08)	1.62(0.11)	1.90(0.12)	4.40(0.14)	5.53(0.20)	7.74(0.31)
Cr ₂ O ₃	0.05(0.05)	0.05(0.06)	0.03(0.04)	0.06(0.07)	0.05(0.07)	0.04(0.03)	0.06(0.06)	0.08(0.10)	0.74
NiO	0.06(0.06)	n. a.	n. a.	0.07(0.06)	0.04(0.05)	0.01(0.02)	0.02(0.03)	n. a.	n. a.
ZnO	0.06(0.08)	0.06(0.07)	N. a	n. a.	n. a.	0.09(0.09)	0.03(0.05)	n. a.	n. a.
P ₂ O ₅	n. a.	n. a.	0.02(0.04)	0.03(0.05)	0.04(0.06)	0.18(0.12)	0.01(0.02)	n. a.	n. a.
SO ₃	n. a.	0.04(0.05)	0.02(0.03)	0.01(0.02)	0.02(0.03)	0.05(0.06)	0.03(0.06)	n. a.	n. a.
F	0.27(0.24)	0.13(0.12)	0.26(0.27)	0.25(0.19)	0.22(0.23)	0.63(0.18)	0.33(0.10)	n. a.	n. a.
Cl	0.02(0.02)	0.04(0.03)	0.06(0.06)	0.07(0.04)	0.10(0.04)	0.40(0.06)	0.14(0.05)	0.15(0.06)	0.05(0.04)

Numerals in parentheses show average deviations in the concentrations, n.a. means not analyzed, * number of analyses.

gioclase in the process of dissolution–crystallization (Johannes, 1989; Acosta-Vigil et al., 2006).

Potassium feldspar in the products of run MK6-12 (Fig. 4d) contains 1.5–2.1 wt % Na₂O and up to 1 wt % CaO. It cannot be ruled out that the presence of CaO is explained by glass inclusions in this feldspar.

MELT COMPOSITIONS

All newly formed associations in the run products with H₂O–CO₂–NaCl and H₂O–CO₂–KCl fluids at 850°C are accompanied by glasses (quenched melts). The run products contain melts of two structural types: (1) small melt portions in association with decomposition products of cordierite and (2) wide melt pools that are usually constrained to “tonalitic” domains in the rock or to contacts between “tonalitic” and “pelitic” domains. These structural differences are correlated with compositional differences of the melts. In the binary diagrams in Fig. 8, these differences are demonstrated for melts in the products of runs MN6-14 and MK6-10. As expected, at similar SiO₂ concentrations, the melts in association with cordierite decomposition products bear higher Al₂O₃ concentrations (higher by 1–2 wt %) than melts in the wide pools. The melts among the replacement products of cordierite are commonly poorer in K₂O and Na₂O, as is most clearly seen in sample MK6-10 (Fig. 8) and is likely explained by that the glass coexists with abundant biotite. The presence of biotite may also explain the relatively low (MgO + FeO) concen-

trations of melts found in association with cordierite replacement products as compared to melts in the wide pools (Fig. 8). It is worth mentioning that the melts of both types contain similar CaO concentrations, likely because of active Ca transfer from plagioclase by fluid interacting with the rock.

Figure 8 shows that the melts whose small portions occur among the cordierite decomposition products define more compact composition fields than those of melts in the wide pools, whose compositional variations are broader. The compositional fields of these melts usually show negative correlations between the SiO₂ concentrations and those of other major components (Fig. 8). This points to different proportions of the “quartz” constituent” of these melts. We assume that the average compositions of melts in the wide pools may more accurately reflect the compositions of the melts that were the closest to equilibrium under the experimental conditions. In view of this, below we discuss the compositions of melts in the wide pools (Table 6).

In experiments with fluids containing relatively low starting concentrations of salts, these melts are close to rhyolite (granite) in composition, 70–76 wt % SiO₂, and show A/CNK > 1.0 and A/NK > 1.0 (Frost et al., 2001; Clemens et al., 2011; Chappell, 1999; Chappell et al., 2012), which corresponds to the field of peraluminous granites (Fig. 9a). Their MALI index (Frost et al., 2001) indicates that the melts affiliate with the calcic and calc–alkaline types (Fig. 9b). The overwhelming majority of the composition points of these

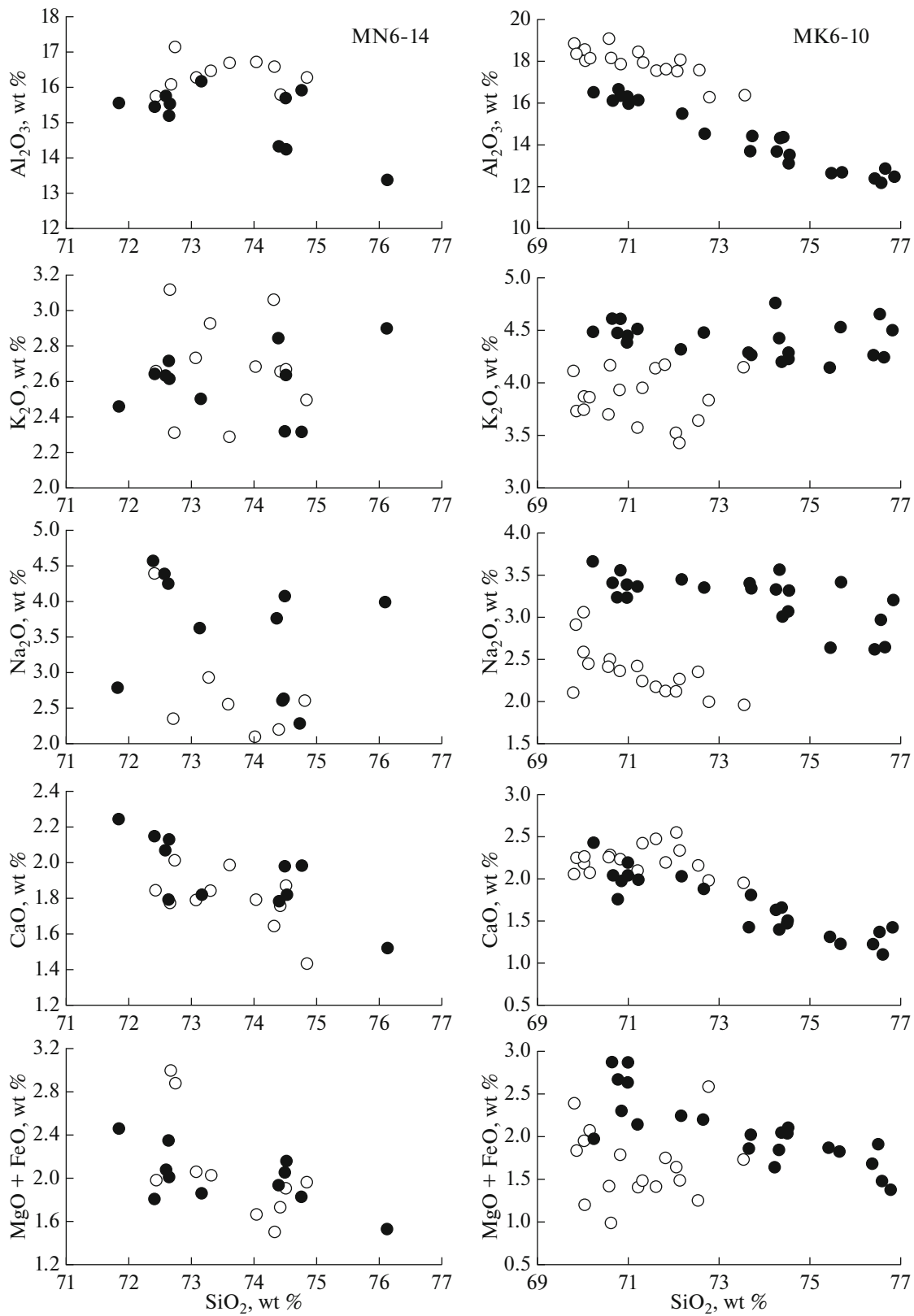
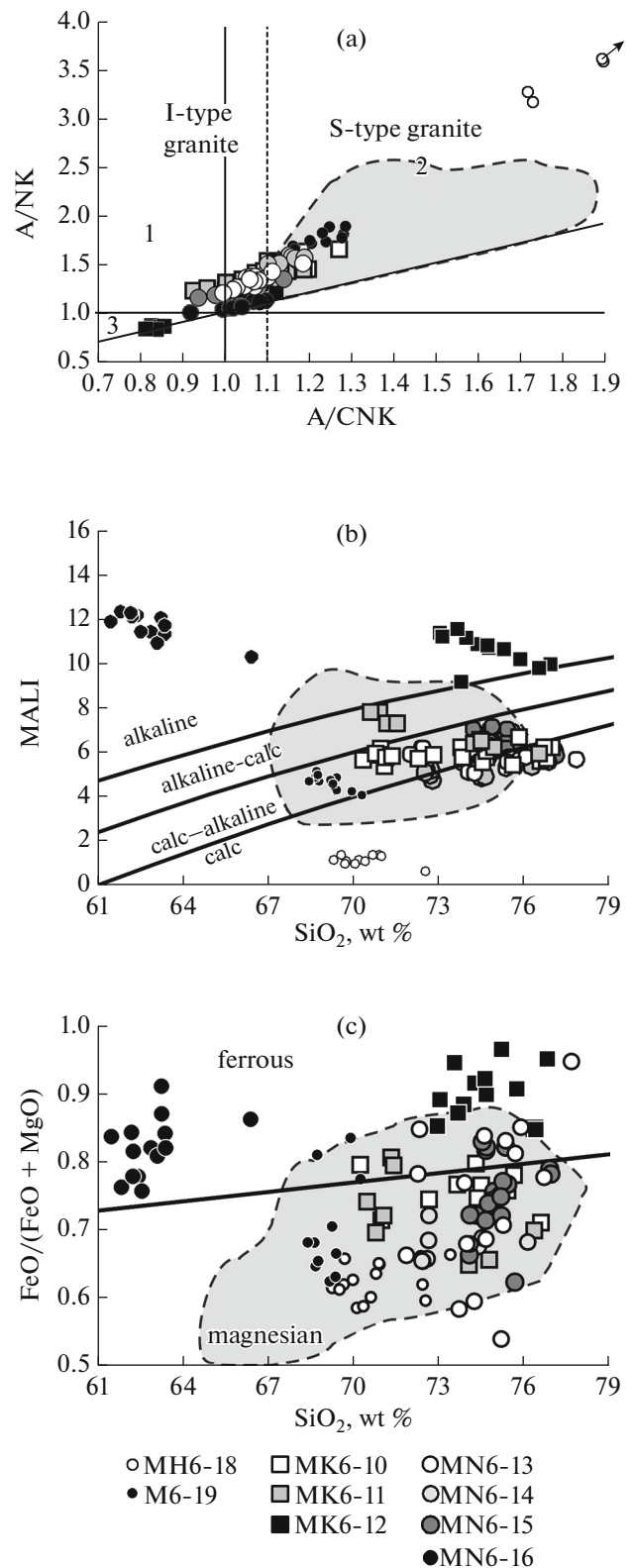


Fig. 8. Comparison of the compositions of the quenched melts produced in small amounts among the decomposition products of cordierite (open circles) and extensive melt pools (solid circles) in the products of runs MN6-14 and MK6-10 (Table 2).

Fig. 9. Characteristics of melts in the run products. (a) A/CNK–A/NK diagram; the vertical solid line at A/CNK = 1.0 is the boundary line between the fields of (1) metaluminous and (2) peraluminous (plumasic) granites (Frost et al., 2001; Clemens et al., 2011; Chappell et al., 2012); the vertical dashed line at A/CNK = 1.1 is the boundary line between the fields of I- and S-type granites (Chappell and White, 2001; Chappell et al., 2012); the horizontal solid line at A/NK = 1.0 is the boundary line between the fields of (1) metaluminous and (3) apatitic granites (Frost et al., 2001); the slant solid line corresponds to equal A/CNK and A/NK values; the arrow points to the field of the composition points of melts in run MH-18, which was conducted with H₂O fluid (Table 2). (b) MALI–SiO₂ diagram; solid lines separate calc, calc-alkaline, alkaline-calc, and alkaline granitoids, according to (Frost et al., 2001). (c) SiO₂–FeO/(FeO+MgO) diagram; the solid line separates ferrous and magnesian granitoids, according to (Frost et al., 2001). In all diagrams, gray fields contoured with dashed lines corresponds to the composition field of melts derived by melting various metapelites under pressures of 500–1500 MPa with or without H₂O fluid (Patino Douce and Johnston, 1991; Patino Douce and Harris, 1998; Pickering and Johnston, 1998; Koester et al., 2002).

melts fall within the field of magnesian granites (Fig. 9c). In runs MN6-16 and MK6-12, conducted with fluids with the highest NaCl and KCl concentrations, respectively, the compositions of the melts are shifted toward the alkaline region (Fig. 9b). These melts contain <1 wt % CaO. The potassic melts bear the lowest Al₂O₃ concentrations (<13 wt %), and their composition points plot within the field of peralkaline granites (Fig. 9a). The relations between the SiO₂ concentrations (62–64 wt %) and MALI indexes (11–12 wt %) of the sodic melts of run MN6-16 correspond to trachyte (Fig. 9b), but the rocks are enriched in Al₂O₃ (up to 20–21 wt %). The peralkaline melts of runs MN6-16 and MK6-12 are noted for high Fe# and plot within the field of Fe-rich granitoids (Fig. 9c).

The composition of the melts depends on the concentrations of alkalis in the starting fluid (Figs. 10a–10e). The K₂O/Na₂O ratios of melts in the presence of KCl-bearing fluid is always greater than 1, increases with increasing KCl concentration in the fluid, and reaches 2.5–2.8 in melts from run MK6-12 (Fig. 10a). This ratio of melts generated in the presence of H₂O–CO₂–NaCl fluid is smaller than 1 and decreases to 0.17–0.18 in the melts of run MN6-16, which was conducted at the maximum NaCl concentration in the fluid (Fig. 10a). Thereby the alkalinity of melts in both experimental series increases with increasing salt concentration in the fluid (Fig. 10b), while the CaO concentration simultaneously decreases (Fig. 10c). The Al₂O₃ concentrations of the melts generally vary very insignificantly and are similar for melts of both experimental series at $X_{\text{salt}} < 0.015$ but change in the opposite manner at higher salt concentrations (Fig. 10d). Nevertheless, melts in runs with H₂O–CO₂–KCl fluid are obviously prone to shift toward



lower A/CNK ratios with increasing salt concentration in the fluid (Fig. 10e). No such tendency was detected in melts from runs with H₂O–CO₂–NaCl fluid (Fig. 10e).

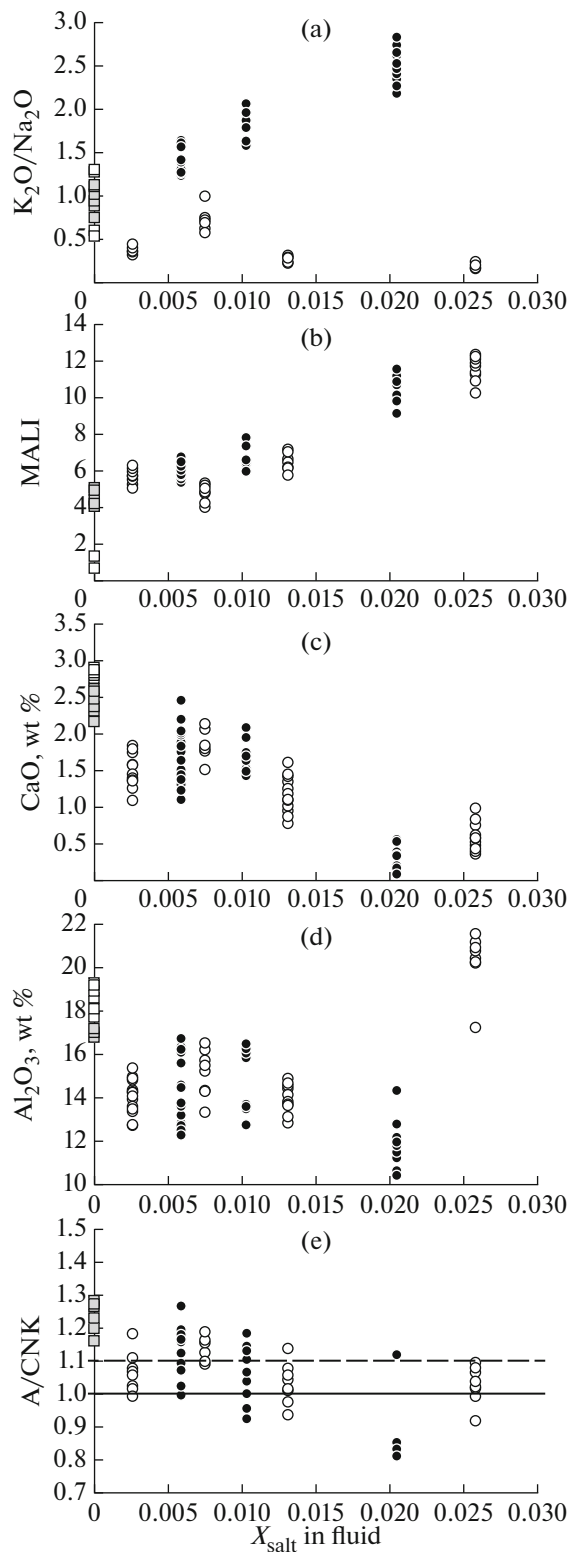


Fig. 10. Dependences of some compositional parameters of the melts [(a) K_2O/Na_2O ; (b) MALI; (c) CaO, wt %; (d) Al_2O_3 , wt %; (e) A/CNK] on the concentrations of KCl (open circles) or NaCl (solid circles) in the fluids. Open squares correspond to melts in the presence of H_2O fluid, gray squares are melts in the presence of H_2O-CO_2 fluid.

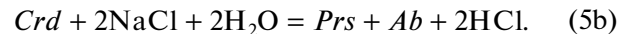
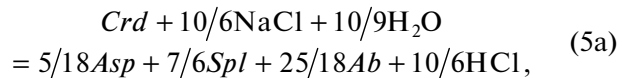
All melts produced by partial melting of metapelite in the presence of H_2O-CO_2-KCl and H_2O-CO_2-NaCl fluids contain Cl, whose concentrations never exceed 0.2 wt % (Table 6), with the only exception for melts from run MN6-16, which contain as much as 0.45 wt % Cl (Table 6). It is hard to estimate how Cl concentrations differ in the melts, because these concentrations broadly vary even in glasses in a single experimental sample (Table 6). The melts contain F, because the starting biotite and apatite in sample PET-5 contained this element.

The melts produced by partial melting of the metapelite in the presence of H_2O and H_2O-CO_2 fluids notably differ from the melts generated in the presence of salt-bearing fluids (Figs. 9a–9c, 10a–10e). These melts are rich in Al_2O_3 and CaO and plot within the fields of peraluminous magnesian calcic and calc-alkaline granitoids (Figs. 9a–9c). The melts generated in the presence of H_2O fluid are richer in these components than the melts produced in the presence of H_2O-CO_2 fluid and show high A/CNK (up to 2.3) and A/NK (up to 6.0) ratios and low MALI values (Figs. 9a, 9b).

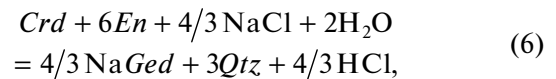
DISCUSSION

Mineral Indicators of Interaction between Metapelite and Fluid Containing Alkali Chlorides

Phases indicative of the interaction of the metapelite of sample PET-5 with H_2O-CO_2-NaCl fluids are Na-bearing biotite and gedrite. These phases are usually found in association with spinel and albite (Figs. 3e, 3f). Biotite containing the aspidolite (*Asp*) and/or preiswerkite (*Prs*) components can be formed after cordierite in the presence of NaCl-bearing fluid by the reactions



Sodic gedrite can be generated at contacts between cordierite and orthopyroxene by the reaction



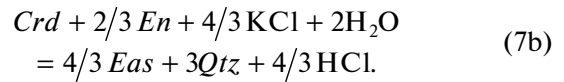
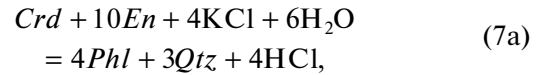
where *NaGed* is $NaMg_6Al_3Si_6O_{22}(OH)_2$ (an end member intermediate between $NaAl_5$ and $NaAl$ in Fig. 8b). The origin of albite and quartz according to reactions (5a), (5b), and (6) may likely be associated with the generation of melt, which is found together with the products replacing the cordierite.

Trioctahedral micas rich in Na₂O and contain the aspidolite and/or preiswerkite components (see Visser et al., 1999 for a review of finds of these minerals) are uniquely rare in metapelite associations. Magnesian biotite containing up to 1.0 wt % Na₂O was found in metapelites in western Greenland (Grew et al., 1987). The mica was found in association with B-bearing kornerupine, cordierite, sapphirine, plagioclase, spinel, and corundum. The gedrite in association with these minerals contains 2 wt % Na₂O. These associations are thought (Grew et al., 1987) to have been formed because B-bearing fluid containing salts has occurred at the metamorphic peak at 700–800°C and 500 MPa. Such fluids could likely be responsible for the origin of Na₂O-rich biotite (1–2 wt % Na₂O) and preiswerkite in association with Cl-bearing scapolite, tourmaline, plagioclase, and apatite in metapelites in contact with gabbro boudins in the Bamble Sector, Norway (Visser et al., 1999; Touret and Nijland, 2013). These data are consistent with the result of our experiments, which show that Na₂O concentration in the biotite is a function of NaCl concentration in the fluid, and the fluids containing as little as 1–2 mol % NaCl are able to produce biotite of the aspidolite–preiswerkite series (Fig. 6b).

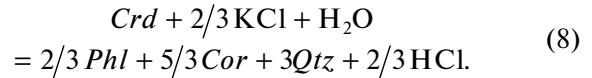
In contrast to Na-bearing biotite, Na-gedrite is widely spread in amphibolite- and granulite-facies metapelites and seems to remain stable up to a temperature of 900°C and may be even higher (Tsunogae et al., 2007; Kanazawa et al., 2009). Our experiments have shown that, at constant *T* and *P*, the concentration of Na₂O in gedrite depends on NaCl concentration in the fluid, and this can be used to evaluate concentrations of salt components during metasomatic processes associated with metamorphism. Following to detailed analysis of gedrite-bearing associations in metapelites in the eastern Ghats, India, Dasgupta et al. (1999) concluded that Na-gedrite (containing up to 1.8–2.5 wt % Na₂O) and its associations with albite were indicators of Na activity in the fluid that interacted with the rock along shear-zones at 750–800°C and 6 MPa, i.e., parameters close to those of our experiments. The results of the experiments demonstrate that a concentration of <1 mol % NaCl in H₂O–CO₂ fluid is sufficient under these *P* and *T* for gedrite with the aforementioned Na₂O concentration to crystallize. It was suggested (Dasgupta et al., 1999) that a further increase in the Na₂O concentration (which can be paralleled with an increase in the salt concentration of the fluid) should destabilize Na-gedrite and produce the *Opx* + *Ab* assemblage. No such assemblage was reproduced in the experiments: the highest NaCl concentration stabilized Na-biotite, a mineral whose possible origin was neglected in (Dasgupta et al., 1999).

According to Korzhinskii (1962), the dominant product of interaction between metapelites and K-bearing fluids at a relatively high H₂O chemical potential is biotite. This conclusion is validated by experiments.

The origin of biotite with the replacement of cordierite and orthopyroxene (Fig. 4a) is described by the reactions



Cordierite replacement by biotite is associated with the origin of additional phases, such as corundum (Figs. 4b, 4d) and, to a lesser extent, spinel

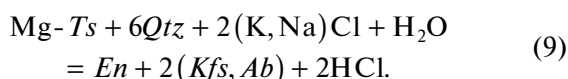


Potassium feldspar is associated with the replacement products of cordierite and orthopyroxene only at the highest KCl concentration in the fluid (run MK6-12, Fig. 4d). At a temperature of 850°C, potassium feldspar coexists with biotite, corundum, and small amounts of melt. However, pilot experiments at 800°C have shown that no potassium feldspar is present among the cordierite replacement products at a KCl concentration in the fluid as in run MK6-12. The amount of biotite in the cordierite replacement products increases and neither corundum nor melt are formed. Hence, potassium feldspar can be formed by reactions between cordierite and H₂O–CO₂–KCl fluid only at relatively high temperature and/or a high activity of potassic component in the fluid. Potassium feldspar is indeed only rarely identified among the products of cordierite replacement by associations with biotite in metapelites. For example, when cordierite is replaced by the *Bt* + *Sil* (*Ky*) + *Qtz* assemblage in metapelites in the Southern Marginal Zone of the Limpopo granulite complex in South Africa, potassium feldspar is absent from this association (van Reenen, 1986; Koizumi et al., 2014; Safonov et al., 2014b) because of the relatively low temperatures of these reactions (<700°C).

In addition to reactions forming new phase associations, the interaction of metapelite of sample PET-5 with H₂O–CO₂–NaCl and H₂O–CO₂–KCl fluids is associated with systematic changes in the composition of the starting minerals of the rock, and this is reflected in their zoning. An example of this is displayed in Fig. 4c, which shows newly formed outer zones of the biotite and orthopyroxene. The biotite produced by reactions of cordierite and orthopyroxene with H₂O–CO₂–NaCl and H₂O–CO₂–KCl fluid is characterized by a low TiO₂ concentration (Table 4) in spite of the high enough temperature of the experiments. When the primary Ti-bearing biotite is replaced by newly formed biotite, TiO₂ concentration in the latter is much lower. This feature can be utilized as a criterion for detecting biotite produced by metasomatic reactions between metapelite assemblages and fluids. This can be illustrated by the example of

metapelites in the rehydration zone of the Southern Marginal Zone of the Limpopo granulite complex in South Africa, in which biotite replacing cordierite, orthopyroxene, and early Ti-bearing biotite is poor in TiO₂. A low TiO₂ concentration in biotite is commonly interpreted as an indication that the biotite crystallized at relatively low temperatures. However, our experiments demonstrate that biotite poor in TiO₂ can also be formed at relatively high temperatures via replacing minerals devoid of TiO₂, when these minerals react with fluids containing salt components.

When H₂O-CO₂-NaCl and H₂O-CO₂-KCl interact with the primary orthopyroxene, it loses Al₂O₃ (Fig. 5, Table 3), in contrast to the effect of H₂O and H₂O-CO₂ fluids, which results in a significant increase in Al₂O₃ concentrations in the newly formed orthopyroxene as compared to the starting one (Fig. 5, Table 3). A decrease in Al₂O₃ concentration in orthopyroxene at its interaction with fluid containing alkali chloride components reflects the reaction



The (Kfs, Ab) component is represented here by granite melt. Reaction (9) is similar to those suggested by various researchers to account for the systematic decrease in Al₂O₃ concentration in orthopyroxene during the development of charnockite associations in mafic and intermediate rocks (Perchuk and Gerya, 1993; Perchuk et al., 2000, 2004; Harlov et al., 1998; Franz and Harlov, 1998; Safonov et al., 2012; Rajesh et al., 2013; Safonov and Aranovich, 2014). In the experimental products, the association of low-Al orthopyroxene and melt was formed only in “tonalitic” domains of the rock, whereas the Al₂O₃ concentration in relics of the starting orthopyroxene in “pelitic” domains does not show such variations. In the presence of cordierite, orthopyroxene is replaced by biotite or gedrite (Figs. 3b, 3c, 4a), and no zoning develops in the relics, which corresponds to reactions (6) and (7a, 7b). This means that reaction (9) in “pelitic” domains of the starting rock is metastable with respect to reactions (6) and (7a, 7b). Indeed, the assemblage of Al₂O₃-poor orthopyroxene and alkali feldspars in the presence of other aluminous phases is rare in metapelites. Associations of orthopyroxene containing less than 0.5 wt % Al₂O₃ with alkali feldspar, sapphirine, spinel, and corundum in metapelites (*Bt* + *Sil* + *Qtz* + *Kfs* + *Pl*) were found, for example, in the Hauglandsvatn area, Bamble Sector, Norway (Nijland et al., 1998). The abundance of brine inclusions in the leucosome associated with these assemblages suggests that aqueous salt fluids were actively involved in processes that formed these unique mineral assemblages in the original metapelites at 752 ± 34°C and 710 ± 40 MPa (Nijland et al., 1998). The possibility of the origin of such phases as corundum and spinel in asso-

ciation with alkali feldspar and granite melt when metapelite interacts with H₂O-CO₂-salt fluid has been demonstrated by our experiments (Figs. 3c, 4d).

Reactions (5)–(8) describe how “pelitic” domains are transformed in the original metapelite PET-5. Its “tonalitic” (i.e., containing plagioclase) domains are characterized by reactions analogous to those identified when tonalitic gneiss interacts with H₂O-CO₂-salt fluid (Safonov et al., 2014a). Peritectic reaction (2) (Fig. 3a) is typical of melting processes of biotite-bearing tonalitic systems with the involvement of H₂O, H₂O-CO₂, or H₂O-CO₂-salt fluids containing low salt concentrations (Gardien et al., 2000; Safonov et al., 2014a). The mineral assemblages produced during the incongruent melting of biotite with plagioclase and quartz in the presence of H₂O-CO₂-NaCl fluid evolve from *Opx* + *Amph* + *melt* in run MN6-13 to *Amph* + *Cpx* + *melt* in run MN6-16 (Fig. 3b), and this evolutionary succession is similar to that detected in experiments on interaction between tonalitic gneiss with H₂O-CO₂-salt fluid whose salt concentration is increased (Safonov et al., 2014a). The association of clinopyroxene and potassium feldspar among the products of interaction of biotite with plagioclase and quartz in metapelite in the presence of H₂O-CO₂-KCl fluid at relatively high KCl concentrations (Fig. 5e) is analogous to the interaction products of tonalitic gneiss with such fluid (Safonov et al., 2014a). The compositional trends of the newly formed minerals are also similar. For instance, an increase in the NaCl concentration is associated with the depletion of the clinopyroxene in Al and its enrichment in the aegirine end member and with enrichment of the newly formed Ca–Na amphibole in winchite.

Simulation of Interaction between Metapelite and H₂O–CO₂–Salt Fluid Using the Pseudosection Method

Experiments demonstrate that metapelite interaction with H₂O-CO₂-NaCl fluid containing up to 2.6 mol % salt notably stabilizes the hydrous phases: Na-bearing biotite and gedrite after cordierite and aluminous orthopyroxene. Analogous interaction between metapelite and H₂O-CO₂-KCl fluid containing less than ~2.0 mol % salt also stabilizes biotite at the expense of these phases. As the KCl concentration is increased to ~2.0 mol %, potassium feldspar is formed in association with biotite. Obviously, the stability field of the micas and amphiboles expands in spite of *a*_{H₂O} < 0.6 in the starting fluid (Table 2), which is explained by an increase in the K and Na activities in the fluid because of the increase in the concentrations of the alkali chloride components. A leading role played by the activities of K and/or Na is obvious from the differences between the interaction products of metapelite with H₂O-CO₂ fluid on the one hand and with H₂O-CO₂-NaCl or H₂O-CO₂-KCl fluids on the

other. Even relatively low concentrations of salt components stabilize biotite and amphiboles.

This conclusion makes it possible to carry out quantitative comparative analysis of reactions and mineral assemblages of metapelite interacting with H₂O–CO₂–salt fluids by simulating the phase relations in $\log(a_{\text{H}_2\text{O}}) - \log(a_{\text{K}_2\text{O}})$ and $\log(a_{\text{H}_2\text{O}}) - \log(a_{\text{Na}_2\text{O}})$ space, as was done to tonalitic gneiss in (Safonov et al., 2014a). The aforementioned parameters present a relative scale that makes it possible to predict mutual effects of the activities of alkali components on mineral assemblages. At known Cl and CO₂ activities, calculated activities of K₂O and Na₂O can be translated into activities of corresponding salt components (Safonov and Aranovich, 2014). The simulations were performed by minimization of the Gibbs free energy with the PERPLE_X software (Connolly, 2005) for a system of given (specified) composition. The assumed standard properties of alkali components were those of solid K₂O and Na₂O from the NIST database. The simulations were conducted with the standard thermodynamic properties from the database (Holland and Powell, 2011) and the following mixing models of solid solution recommended in PERPLE_X (http://www.perplex.ethz.ch/PerpleX_solution_model_glossary.html): Opx(HP) for orthopyroxene; hCrd for hydrous cordierite, Bio(TCC) for Ti-bearing biotite, oAmph(DP) for Na-bearing amphibole of the anthophyllite–gedrite series, Sp(HP) for spinel, and melt(HP) for silicate melt in the NCKFMASH system.

As seen in Figs. 11a and 11b, reactions describing the transformations of the metapelite have gentle slopes in $\log(a_{\text{H}_2\text{O}}) - \log(a_{\text{K}_2\text{O}})$ and $\log(a_{\text{H}_2\text{O}}) - \log(a_{\text{Na}_2\text{O}})$ space, i.e., these reactions are more strongly dependent on the activities of alkali components than H₂O. The mineral assemblages simulated by Gibbs free energy minimization are similar to those in the experimental products. For example, an increase in the Na₂O activity leads to the disappearance of, first, cordierite and the origin of an association of biotite with less aluminous orthopyroxene and sodic plagioclase. Then Na-bearing amphibole joins this assemblage (Fig. 11a). This mineral is widespread in the experimental products (Figs. 3b, 3c). At relatively high $\log(a_{\text{Na}_2\text{O}})$, PERPLE_X predicts the origin of the Na-phlogopite component in the biotite and the crystallization of pargasite amphibole, which was also identified in the experimental products and was formed by reactions involving plagioclase (Fig. 3a). An increase in the K₂O activity results, first, in cordierite replacement by biotite and then in the decomposition of orthopyroxene (Fig. 11b). This succession is also identified in the experimental products. Newly formed biotite was found in runs MK6-9 and MK6-10, and this orthopyroxene is poorer in Al₂O₃. An increase in the KCl concentration in run MK6-11 results in the development of biotite rims between cordierite and ortho-

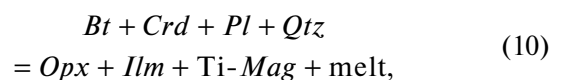
pyroxene, but no zoning develops thereby in the orthopyroxene (Fig. 4a). The diagram in Fig. 11b predicts the origin of diopside, and this was reproduced in run MK6-12 (Fig. 4e).

A noteworthy feature of diagrams in Figs. 11a and 11b is the configurations of the solidi of the rocks with minima in $a_{\text{H}_2\text{O}}$. Analysis of the mineral assemblages shows that regions around these minima correspond to $\log(a_{\text{K}_2\text{O}})$ and $\log(a_{\text{Na}_2\text{O}})$ values above which quartz is absent from the subsolidus assemblages, but these instead contain alkali feldspar. A further increase in the activities of alkali components results in the onset of melting at higher $a_{\text{H}_2\text{O}}$. Since an increase in the activities of alkali components is associated with a decrease in the water activity (see Table 2 for $a_{\text{H}_2\text{O}}$ values), this configuration of the solidi means that the intensity of melting decreases with increasing intensity of metasomatic transformations.

Melting Specifics and Variations in the Melt Composition

All reactions in the metapelite in the presence of H₂O, H₂O–CO₂, H₂O–CO₂–NaCl, and H₂O–CO₂–KCl fluids at 600 MPa and 850°C describe incongruent melting with the generation of various melt volumes. The compositions of these melts are controlled, first, by the microassociations from which the melts are derived and, second, by the peritectic phases in equilibrium with the melts.

Thanks to the active involvement of cordierite in melting reactions along with other phases of the metapelite, the rhyolitic melts derived in the presence of H₂O fluid (Table 2, run MN6-18) acquire very high A/CNK and A/NK ratios but low MALI and FeO/(FeO + MgO) values (Figs. 9a–9c, 10a–10e). Such A/CNK values (>1.6) are rare among S-type granites (Chappell and White, 2001; Chappell et al., 2012), in whose field the composition points of melts from run MN6-18 plot (Fig. 9a). The parameters of melts in run MN6-18 notably differ from those of melts derived at both dehydration and hydrous melting of biotite–muscovite metapelitic associations within a broad pressure range (e.g., Patino Douce and Johnston, 1991; Patino Douce and Harris, 1998; Pickering and Johnston, 1998). Melts whose compositions were most closely similar to our melts were obtained in experiments (Koester et al., 2002) on dehydration melting of cordierite gneiss at 500 MPa. However, even these melts show lower A/CNK and A/NK ratios than those of melts in run MN-18. The melting reaction suggested in (Koester et al., 2002) is



and is similar to reaction (1). This reaction also produces orthopyroxene containing up to 8.8 wt % Al₂O₃, which is similar to the orthopyroxene in the products

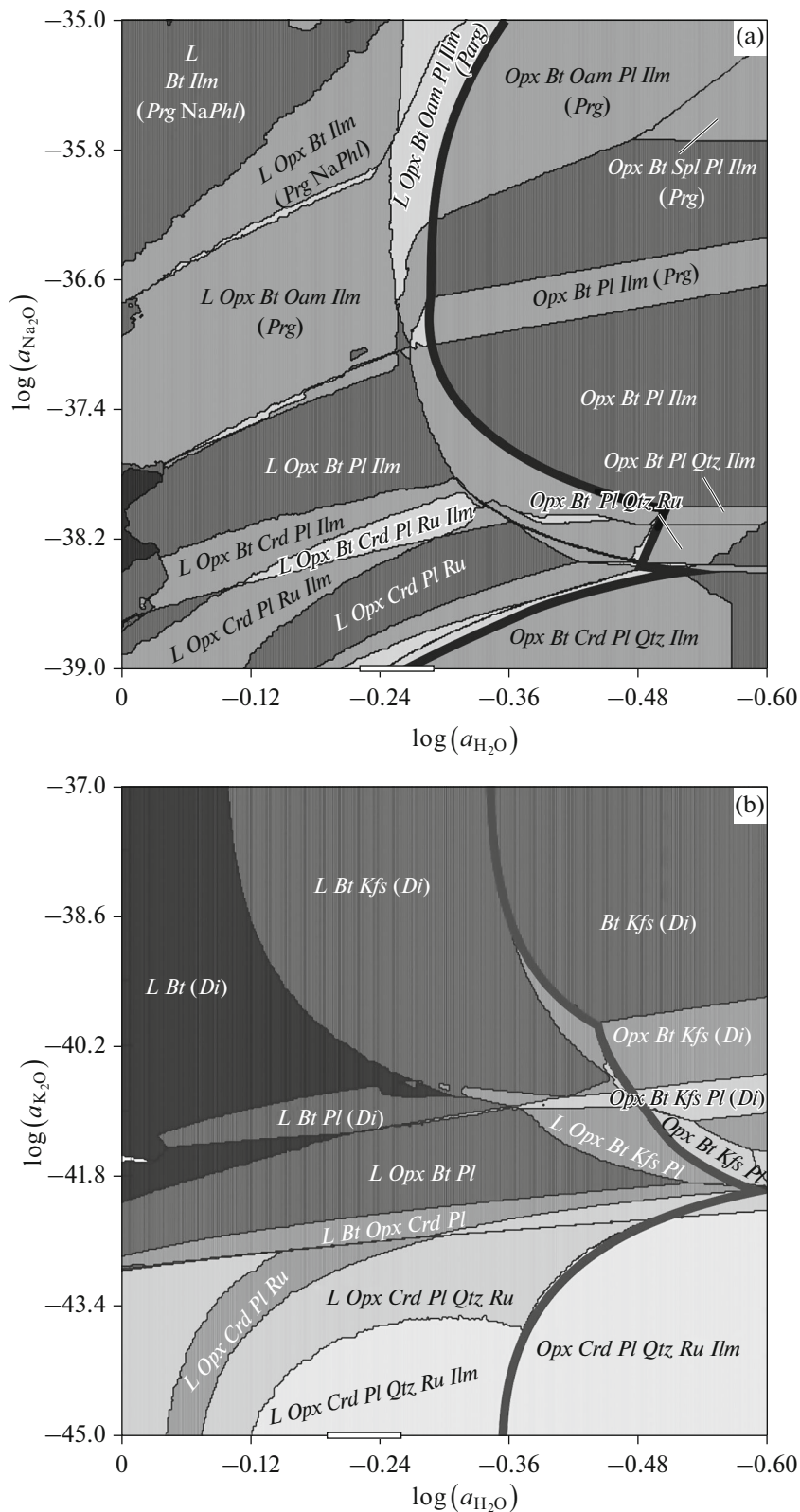
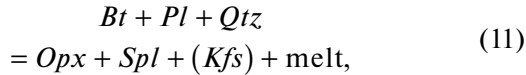


Fig. 11. Pseudosections in (a) $\log(a_{\text{H}_2\text{O}})$ – $\log(a_{\text{Na}_2\text{O}})$ and (b) $\log(a_{\text{H}_2\text{O}})$ – $\log(a_{\text{K}_2\text{O}})$ diagrams calculated for the composition of sample PET-5 (Table 1) at 850°C and 600 MPa. The diagrams show principally important phase fields. Heavy solid lines are rock solidi depending on the foregoing parameters. White bars on the $\log(a_{\text{H}_2\text{O}})$ axes denote the ranges of H_2O activity calculated for the starting fluid composition in the experimental runs (Table 2).

of run MN6-18 (Table 3). The likely reason for the origin of spinel (Fig. 2a) among the products of run MN6-18 was higher Al_2O_3 concentration in the metapelite of sample PET-5 (Table 1) compared to that in the rock utilized in the experiments (Koester et al., 2002). Spinel could also be formed by a reaction not involving cordierite



as was noted in (Vielzeuf and Montel, 1994) for experiments on dehydration melting of the association $Bt + Pl + Qtz$ at pressures of 400–600 MPa. At a similar Mg-number of the starting association in the experiments (Vielzeuf and Montel, 1994), spinel crystallized in them at temperatures higher than 850°C, and garnet was stable at lower temperatures. The presence of H_2O in run MN6-18 or $\text{H}_2\text{O}-\text{CO}_2$ fluid in run M6-19 (Table 2) decreased the temperature at which spinel, aluminous orthopyroxene, and melt coexisted.

Assemblages with magnesian ($X_{\text{Mg}} > 0.60$) aluminous orthopyroxene and spinel are typical of certain so-called Mg-Al granulites. The crystallization temperatures of these associations are often evaluated at more than 900°C, as is typical of ultrahigh-temperature (UHT) metamorphism (e.g., Kelsey and Hand, 2015). Some researchers are prone to think that Mg-Al associations can be formed as residuals after partial melting of “usual” biotite-bearing metapelitic protoliths (e.g., Bose et al., 2000). This hypothesis was, however, questioned (e.g., Kelsey and Hand, 2015) on the ground that the redistribution of relatively small MgO and FeO amounts into granite melt at partial melting cannot appreciably increase the Mg mole fractions of the residual minerals, even in spite of the fact that the $\text{FeO}/(\text{FeO} + \text{MgO})$ ratio of the melt is higher than in the residue. This conclusion nevertheless holds for small melt volumes derived via dehydration melting. As shown by runs MH6-18 and M6-19, the amount of melt drastically increases in the presence of H_2O and $\text{H}_2\text{O}-\text{CO}_2$ fluids, and the effect of FeO and MgO distribution between the melt and residue is significant. In other words, the Mg mole fraction of the peritectic orthopyroxene and spinel should depend on the degree of melting. Such a dependence was indeed detected at melting of metapelite of sample PET-5. In run MH6-18 (with the maximum degree of melting), the orthopyroxene has $X_{\text{Mg}} = 0.79-0.82$ and the spinel has $X_{\text{Mg}} = 0.63-0.65$ (Table 3), while in run M6-19 at lower degree of melting, X_{Mg} decrease down to 0.69–0.73 and 0.44–0.46, respectively (Table 3). The increase of the Mg mole fraction of the cordierite undoubtedly depends, first of all, on how much the most magnesian phase (cordierite) is involved in the melting reactions. The Mg–Al association can thus be formed by the local partial melting of “usual” cordierite-bearing granulites in the presence of H_2O or $\text{H}_2\text{O}-\text{CO}_2$ fluids. In the presence of $\text{H}_2\text{O}-\text{CO}_2$ fluids,

which induce a lower degree of melting, these associations can coexist with granite melts with characteristics of S-type granites (Fig. 9a).

The presence of KCl and NaCl in fluids leads to cordierite replacement by associations with biotite and/or amphibole, which are, in turn, stable in the presence of melts. Cordierite is thus removed from the melting reactions, and the total melting of the metapelite is controlled first of all by peritectic reactions of biotite and/or, to a lesser extent, orthopyroxene with plagioclase and quartz. The broad compositional variability of the melts and negative correlations between the concentrations of major oxides and SiO_2 even within a single sample (Fig. 8) highlight the significant effect of the local variations in the bulk composition of the precursor rocks due to variations in its microassociations. Thereby correlations between K_2O and Na_2O concentrations of the melts are either not as strong or even not discernible at all (Fig. 8), because these parameters are controlled by K and Na activities in the equilibrium fluids.

In contrast to peraluminous melts derived in the presence of H_2O and $\text{H}_2\text{O}-\text{CO}_2$ fluids, the composition of melts in the presence of salt-bearing fluids are shifted toward A/CNK values between 1.1 and 1.0, and the melts derived in the presence of $\text{H}_2\text{O}-\text{CO}_2$ -KCl fluid show a tendency toward a further decrease in the A/CNK parameter (Figs. 9a, 10e). Values of A/CNK = 1.1–1.0 are typical of so-called peraluminous granites of type I, whose compositions are overlapped by those of S-type granites (e.g., Chappell, 1999; Clemens et al., 2011; Chappell et al., 2012). In contrast to typical low-Al (A/CNK < 1.0) type-I granites, whose dominant mafic mineral is Ca–Na amphibole, peraluminous I-type granites typically contain biotite (Chappell et al., 2012). Both groups of I-type granites are commonly closely interrelated and occur in the same complexes (Chappell, 1999; Chappell et al., 2012). Analysis of petrochemical and geochemical data shows that low- and high-Al I-type granites can hardly be formed by extensive fractional crystallization of granite magmas (Chappell, 1999). Certain experimental data demonstrate that melting of basalt and basaltic andesite systems with A/CNK < 1.0 is able to produce melts with A/CNK > 1.0 (e.g., Beard and Lofgren, 1991; Sisson et al., 2005), and hence, I-type peraluminous granite melts can be produced with the involvement of peritectic reactions in biotite- and/or amphibole-bearing protoliths at $T > 900^\circ\text{C}$, which produce Ca-pyroxene and Fe–Ti oxides (Clemens et al., 2011; Chappell et al., 2012). The evolutionary trends of these melts from Al-saturated (A/CNK > 1.0) toward Al-undersaturated derivatives is explained by different degrees of the dissolution of calcic pyroxene and, to a lesser extent, also amphibole, in magmas ascending to the surface (Clemens et al., 2011; Chappell et al., 2012).

It was also noted (Chappell and White, 2001) that the values of the A/CNK ratio of peraluminous I-type

granites overlap with the values of the most silicic varieties of S-type granites. Results of our experiments show that I-type peraluminous granites can also be derived from metapelites melted when interacting with H₂O-CO₂-salt fluids. Compositional trends of the melts from varieties with A/CNK > 1.1 (typical of S-type granites) toward rocks with A/CNK = 1.0–1.1 may be caused by an increase in the concentrations of salts in the fluids, and a shift can be induced even by changes in the salt concentrations as small as a few percent (Table 2). Type-I granites with A/CNK = 1.0–1.1 usually bear relatively low (<2 wt %) CaO concentrations (e.g., Chappell et al., 2012). This compositional feature of the melt is in good agreement with experimental results, which display a systematic decrease in the CaO concentration with increasing concentrations of salts in the fluid (Fig. 10c). This is explained by the stabilization of calcic pyroxene and calcic–sodic amphibole, typical minerals of I-type granites, as a result of plagioclase-involving peritectic reactions. In metapelite systems, Ca–Na amphibole (tschermakite) was identified only in the products of experiments (Koester et al., 2002) on the dehydration and hydrous melting of cordierite-bearing gneiss at 1500 MPa. No clinopyroxene has ever been identified among the products of experiments on the melting of metapelites (Patino Douce and Johnston, 1991; Patino Douce and Harris, 1998; Pickering and Johnston, 1998) and metagraywackes (Vielzeuf and Montel, 1994). Neither clinopyroxene nor amphibole crystallize (and are even not preserved) during the melting of a layered metabasite–metapelite source (Skjerlie and Douce, 1995). Obviously enough, calcic phases generally atypical of metapelites were produced in our experiments by reactions between originally heterogeneous rock and fluid. Such local heterogeneities in crustal magma generation regions may cause notable variations in the chemistries of granitic melts derived via various peritectic reactions (e.g., Clemens et al., 2011).

CONCLUSIONS

Our experiments under a pressure of 600 MPa and a temperature of 850°C demonstrate that reactions producing new mineral assemblages in orthopyroxene–cordierite–biotite–plagioclase–quartz metapelite interacting with H₂O-CO₂-NaCl and H₂O-CO₂-KCl fluids are controlled mostly by the K and/or Na activities. The affect of H₂O on these reactions is hard to evaluate based on the results of the experiments because this activity varied within a relatively narrow range (0.599–0.523, Table 2) in our experiments with H₂O-CO₂-NaCl and H₂O-CO₂-KCl fluids. The dominant role of K and Na activities in these reactions is reflected in the stabilization of the newly formed biotite and amphibole after cordierite, aluminous orthopyroxene, and biotite. This is generally analogous to what occurred in our experiments modeling interaction between biotite–amphibole tonalitic gneiss with

H₂O-CO₂-NaCl, H₂O-CO₂-KCl, and H₂O-CO₂-(K,Na)Cl fluids under similar *P–T* parameters (Safonov et al., 2014a). The stabilizing effect of alkali fluid components with respect to hydrous minerals in metapelite is much more obvious because this system is more magnesian, which is favorable for the expansion of the stability fields of biotite and amphiboles.

The decomposition of cordierite and aluminous orthopyroxene with the origin of hydrous phases principally modifies the melting character of the metapelite, which is controlled by peritectic reactions of biotite and orthopyroxene with plagioclase and quartz. The associations of peritectic phases are analogous to those in the biotite–amphibole tonalitic gneiss. Among other things, they lead to the origin of Ca–Na amphibole and clinopyroxene, i.e., phases atypical of metapelites. The compositions of the melts are also highly sensitive to changes in the character of melting and become less aluminous. The compositional trends of the melts from those with A/CNK > 1.1, as is inherent to S-type granites, to those with A/CNK = 1.0–1.1 and even lower in response to an increase in the concentration of the alkali salt components of the fluids can realistically explain relations between various types of granites occurring in the same complexes. The changes in the composition of the granites can be induced by variations in the concentrations of the alkali salt fluid components even as little as a few mole percent, i.e., concentrations typical of crustal fluids.

ACKNOWLEDGMENTS

The authors thank L.Ya. Aranovich and A.V. Giris (Institute of the Geology of Ore Deposits, Petrography, Mineralogy, and Geochemistry, Russian Academy of Sciences) for constructive scientific and editorial criticism. D.A. Varlamov, A.N. Nekrasov, A.A. Viryus, and K.V. Van (Institute of Experimental Mineralogy), Russian Academy of Sciences) are thanked for help with microprobe analysis of run samples. The part of this study dealing with relations between granite magmatism and granulites was financially supported by Russian Science Foundation (project 14-17-00581), and its part related to studying the effects of K and Na activities on reactions at metamorphism was supported by the Russian Foundation for Basic Research, project no. 16-05-00266.

REFERENCES

- Acosta-Vigil, A., London, D., and Morgan, G.B., Experiments on the kinetics of partial melting of a leucogranite at 200 MPa H₂O and 690–800°C: compositional variability of melts during the onset of H₂O-saturated crustal anatexis, *Contrib. Mineral. Petrol.*, 2006, vol. 151, pp. 539–551.
- Aranovich, L.Y. and Safonov, O.G., Halogens in high-grade metamorphism, in *The role of halogens in Terrestrial and Extraterrestrial Geochemical Processes*, Harlov, D.E. and Aranovich, L.Y., Eds., 2017 (in press).

- Aranovich, L.Ya., Zakirov, I.V., Sretenskaya, N.G., and Gerya, T.V., Ternary system H₂O–CO₂–NaCl at high *T–P* parameters: an empirical mixing model, *Geochem. Int.*, 2010, vol. 48, no. 5, pp. 446–455.
- Aranovich, L.Y., Shmulovich, K.I., and Fed'kin, V.V., The H₂O and CO₂ regime in regional metamorphism, *Int. Geol. Rev.*, 1987, vol. 29, pp. 1379–1401.
- Aranovich, L.Y. and Newton, R.C., H₂O activity in concentrated KCl and KCl–NaCl solutions at high temperatures and pressures measured by the brucite–periclase equilibrium, *Contrib. Mineral. Petrol.*, 1997, vol. 127, pp. 261–271.
- Aranovich, L.Y., Newton, R.C., and Manning, C.E., Brine-assisted anatexis: experimental melting in the system haplogranite–H₂O–NaCl–KCl at deep-crustal conditions, *Earth Planet. Sci. Lett.*, 2013, vol. 374, pp. 111–120.
- Aranovich, L.Y., Makhluf, A.R., Manning, C.E., and Newton, R.C., Dehydration melting and the relationship between granites and granulites, *Precambrian Res.*, 2014, vol. 253, pp. 26–37.
- Beard, J. and Lofgren, G., Dehydration melting and water-saturated melting of basaltic and andesitic greenstones and amphibolites at 1, 3 and 6.9 kb, *J. Petrol.*, 1991, vol. 32, pp. 365–402.
- Bose, S., Fukuoka, M., Sengupta, P., and Dasgupta, S., Evolution of high-Mg–Al granulites from Sunkarametta, Eastern Ghats, India: evidence for a lower crustal heating–cooling trajectory, *J. Metamorph. Geol.*, 2000, vol. 18, pp. 223–240.
- Chappell, B.W., Aluminium saturation in I- and S-type granites and the characterization of fractionated haplogranites, *Lithos*, 1999, vol. 46, pp. 535–551.
- Chappell, B.W. and White, A.J.R., Two contrasting granite types: 25 years later, *Austral. J. Earth Sci.*, 2001, vol. 48, pp. 489–499.
- Chappell, B.W., Bryant, C.J., and Wyborn, D., Peraluminous I-type granites, *Lithos*, 2012, vol. 153, pp. 142–153.
- Clemens, J.D., Stevens, G., and Farina, F., The enigmatic source of I-type granites: the peritectic connexion, *Lithos*, 2011, vol. 126, pp. 174–181.
- Connolly, J.A.D., Computation of phase equilibria by linear programming: a tool for geodynamic modeling and its application to subduction zone decarbonation, *Earth Planet. Sci. Lett.*, 2005, vol. 236, pp. 524–541.
- Dasgupta, S., Sengupta, P., Sengupta, Pr., et al., Petrology of gedrite-bearing rocks in mid-crustal ductile shear zones from the Eastern Ghats Belt, India, *J. Metamorph. Geol.*, 1999, vol. 17, pp. 765–778.
- Franz, L. and Harlov, D.E., High-grade K-feldspar veining in granulites from the Ivrea–Verbano zone, northern Italy: fluid flow in the lower crust and implications for granulite facies genesis, *J. Geol.*, 1998, vol. 106, pp. 455–472.
- Frost, B.R., Barnes, C.G., Collins, W.J., et al., A geochemical classification for granitic rocks, *J. Petrol.*, 2001, vol. 42, pp. 2033–2048.
- Gardien, V., Thompson, A.B., and Ulmer, P., Melting of biotite + plagioclase + quartz gneisses: the role of H₂O in the stability of amphibole, *J. Petrol.*, 2000, vol. 41, pp. 651–666.
- Gilbert, F., Guillaume, D., and Laporte, D., Importance of fluid immiscibility in the H₂O–NaCl–CO₂ system and selective CO₂ entrapment in granulites: experimental phase diagram at 5–7 kbar, 900°C and wetting textures, *Eur. J. Mineral.*, 1998, vol. 10, pp. 1109–1123.
- Grew, E.S., Herd, R.K., and Marquez, N., Boron-bearing kornorupine from fiskenaeset, west Greenland: a reexamination of specimens from the type locality, *Mineral. Mag.*, 1987, vol. 51, p. 695.
- Hansen, E., Ahmed, K., and Harlov, D.E., Rb depletion in biotites and whole rocks across an amphibolite to granulite facies transition zone, Tamil Nadu, South India, *Lithos*, 2002, vol. 64, pp. 29–47.
- Harlov, D.E., Fluid induced dehydration of mafic lower crust from amphibolite to granulite facies: nature and experiment, *Amer. Geophys. Union, Fall Meeting 2004*, vol. 85, p. 47.
- Harlov, D.E., *Petrological and experimental application of REE- and actinide-bearing accessory minerals to the study of Precambrian high-grade gneiss terranes, Origin and Evolution of Precambrian High-Grade Terrains, with Special Emphasis on the Limpopo Complex in Southern Africa*, Van Reenen D.D., Kramers J.D., McCourt S., Perchuk L.L., Eds., *Geol. Soc. Am. Mem.*, 2011, vol. 207, pp. 13–24.
- Harlov, D.E. and Förster, H.-J., High-grade fluid metasomatism on both a local and regional scale: the Seward Peninsula, Alaska and the Val Strona di Omegna, Ivrea–Verbano zone, northern Italy. Part I: petrography and silicate mineral chemistry, *J. Petrol.*, 2002, vol. 43, pp. 769–799.
- Harlov, D.E. and Melzer, S., Experimental partitioning of Rb and K between phlogopite and concentrated (K, Rb)Cl brine: implication for the role of concentrated KCl brines in the depletion of Rb in phlogopite and the stability of phlogopite during charnockite genesis, *Lithos*, 2002, vol. 64, pp. 15–28.
- Harlov, D.E., Hansen, E.C., and Bigler, C., Petrologic evidence for K-feldspar metasomatism in granulite facies rocks, *Chem. Geol.*, 1998, vol. 151, pp. 373–386.
- Harlov, D.E., Van den Kerkhof, A., and Johansson, L., Localized, solid-state dehydration associated with the Varberg charnockite intrusion, SW Sweden, *Precambrian Res.*, 2014, vol. 253, pp. 50–62.
- Hawthorne, F.C., Schindler, M., Abdu, Y., et al., The crystal chemistry of the gedrite-group amphiboles. II. Stereochemistry and chemical relations, *Mineral. Mag.*, 2008, vol. 72, pp. 731–745.
- Heinrich, W., Fluid immiscibility in metamorphic rocks, *Rev. Mineral. Geochem.*, 2007, vol. 65, pp. 389–430.
- Holland, T.J.B. and Powell, R., An improved and extended internally consistent thermodynamic dataset for phases of petrological interest, involving a new equation of state for solids, *J. Metamorph. Geol.*, 2011, vol. 29, pp. 333–383.
- Johannes, W., Melting of plagioclase–quartz assemblages at 2 kbar water pressure, *Contrib. Mineral. Petrol.*, 1989, vol. 103, pp. 270–276.
- Johnson, E.L., Experimentally determined limits for H₂O–CO₂–NaCl immiscibility in granulites, *Geology*, 1991, vol. 19, pp. 925–928.
- Kanazawa, T., Tsunogae, T., Sato, K., and Santosh, M., The stability and origin of sodic gedrite in ultrahigh-temperature Mg–Al granulites: a case study from the Gondwana suture in southern India, *Contrib. Mineral. Petrol.*, 2009, vol. 157, pp. 95–110.
- Kelsey, D.E. and Hand, M., On ultrahigh temperature crustal metamorphism: phase equilibria, trace element

- thermometry, bulk composition, heat sources, timescales and tectonic settings, *Geosci. Front.*, 2015, vol. 6, pp. 311–356.
- Khodorevskaya L.I. Granitization of Amphibolites: 2. Characterization of Physical and Chemical Phenomena Related to Fluid Filtration through a Rock, *Petrology*, 2004, vol. 12, no. 3, pp. 282–295.
- Khodorevskaya, L.I. and Aranovich, L.Ya., Experimental study of amphibole interaction with H₂O–NaCl fluid at 900°C, 500 MPa: toward granulite facies melting and mass transfer, *Petrology*, 2016, vol. 24, no. 3, pp. 215–233.
- Kilink, I.A. and Burnham, C.W., Partitioning of chloride between a silicate melt and coexisting aqueous phase from 2 to 8 kilobars, *Econ. Geol.*, 1972, vol. 67, pp. 231–235.
- Koester, E., Pawley, A.R., Fernandes, L.A., et al., Experimental melting of cordierite gneiss and the petrogenesis of syntranscurrent peraluminous granites in southern Brazil, *J. Petrol.*, 2002, vol. 43, pp. 1595–1616.
- Koizumi, T., Tsunogae, T., and van Reenen, D.D., Fluid evolution of partially retrogressed pelitic granulite from the southern marginal zone of the Neoproterozoic Limpopo Complex, South Africa: evidence from phase equilibrium modeling, *Precambrian Res.*, 2014, vol. 253, pp. 146–156.
- Korikovskiy, S.P. and Aranovich, L.Ya., Charnockitization and enderbitization of mafic granulites in the Porya Bay Area, Lapland Granulite Belt, southern Kola Peninsula: I. Petrology and geothermobarometry, *Petrology*, 2010, vol. 18, no. 4, pp. 320–349.
- Korikovskiy, S.P. and Aranovich, L.Ya., Charnockitization of feldspar-free orthopyroxene–clinopyroxene–phlogopite metaultramafite in the Lapland Granulite Belt, southern Kola Peninsula: compositional trends of rocks and minerals, *P–T* parameters, and fluid regime, *Petrology*, 2015, vol. 23, no. 3, pp. 189–226.
- Korzhinskii, D.S., Role of alkalinity in the formation of charnockite gneisses, *Tr. Vostochno-Sibirsk. Inst. Akad. Nauk SSSR, Ser. Geol.*, 1962, vol. 5, pp. 50–61.
- Larikova, T.L. and Zarakisky, G.P., Experimental modeling of corona textures, *J. Metamorph. Geol.*, 2009, vol. 27, pp. 139–151.
- Manning, C.E., Thermodynamic modeling of fluid–rock interaction at mid-crustal and upper-mantle conditions, *Rev. Mineral. Geochem.*, 2013, vol. 76, pp. 135–164.
- Manning, C.E. and Aranovich, L.Y., Brines at high pressure and temperature: thermodynamic, petrological and geochemical effects, *Precambrian Res.*, 2014, vol. 253, pp. 6–16.
- Markl, G. and Bucher, K., Composition of fluids in the lower crust inferred from metamorphic salt in lower crustal rocks, *Nature*, 1998, vol. 391, pp. 781–783.
- Newton, R.C., Simple-system mineral reactions and high-grade metamorphic fluids, *Eur. J. Mineral.*, 1995, vol. 7, pp. 861–881.
- Newton, R.C. and Manning, C.A., Role of saline fluids in deep-crustal and upper-mantle metasomatism: insights from experimental studies, *Geofluids*, 2010, vol. 10, pp. 58–72.
- Newton, R.C., Smith, J.V., and Windley, B.F., Carbonic metamorphism, granulites and crustal growth, *Nature*, 1980, vol. 288, pp. 45–50.
- Newton, R.C., Aranovich, L.Y., Hansen, E.C., and Vandenheuvell, B.A., Hypersaline fluids in Precambrian deep-crustal metamorphism, *Precambrian Res.*, 1995, vol. 91, pp. 41–63.
- Newton, R.C., Touret, J.L.R., and Aranovich, L.Y., Fluids and H₂O activity at the onset of granulite facies metamorphism, *Precambrian Res.*, 2014, vol. 253, pp. 17–25.
- Nijland, T.G., Touret, J.L., and Visser, D., Anomalously low temperature orthopyroxene, spinel, and sapphirine occurrences in metasediments from the Bamble amphibolite-to-granulite facies transition zone (South Norway): possible evidence for localized action of saline fluids, *J. Geol.*, 1998, vol. 106, pp. 575–590.
- Patino Douce, A.E. and Harris, N., Experimental constraints on Himalayan anatexis, *J. Petrol.*, 1998, vol. 39, pp. 689–710.
- Patino Douce, A.E. and Johnston, A.D., Phase equilibria and melt productivity in the pelitic system: implications for the origin of peraluminous granitoids and aluminous granulites, *Contrib. Mineral. Petrol.*, 1991, vol. 107, pp. 202–218.
- Perchuk, L.L. and Gerya, T.V., *Fluid control of charnockitization*, *Chem. Geol.*, 1993, vol. 175–186.
- Perchuk L.L., Gerya T.V., and Korsman, K., Model of charnockitization of gneiss complexes, *Petrologiya*, 1994, vol. 2, no. 5, pp. 451–480.
- Perchuk, L.L., Safonov, O.G., Gerya, T.V., et al., Mobility of components in metasomatic transformation and partial melting of gneisses: an example from Sri-Lanka, *Contrib. Mineral. Petrol.*, 2000, vol. 140, pp. 212–232.
- Pickering, J.M. and Johnston, D.A., Fluid-absent melting behavior of a two-mica metapelite: experimental constraints on the origin of Black Hills granite, *J. Petrol.*, 1998, vol. 39, pp. 1787–1804.
- Rajesh, H.M., Belyanin, G.A., Safonov, O.G., et al., Fluid-induced dehydration of the Paleoproterozoic Sand River biotite-hornblende gneiss, Central Zone, Limpopo Complex, South Africa, *J. Petrol.*, 2013, vol. 54, pp. 41–74.
- Ravindra-Kumar, G.R., Mechanism of arrested charnockite formation at Nemmara, Palghat region, southern India, *Lithos*, 2004, vol. 75, pp. 331–358.
- Ryabchikov, I.D. and Hamilton, D.L., Possibility of separation of concentrated chloride solutions during crystallization of felsic magmas, *Dokl. Akad. Nauk SSSR*, 1971, vol. 197, pp. 933–937.
- Safonov, O.G., The role of alkalis in the formation of coronitic textures in metamangerites and metaanorthosites from the Adirondack Complex, United States, *Petrology*, 1998, vol. 6, no. 6, pp. 583–602.
- Safonov, O.G. and Aranovich, L.Y., Alkali control of high-grade metamorphism and granitization, *Geosci. Front.*, 2014, vol. 5, pp. 711–727.
- Safonov, O.G., Kosova, S.A., and van Reenen, D.D., Interaction of biotite–amphibole gneiss with H₂O–CO₂–(K, Na)Cl fluids at 550 MPa and 750 and 800°C: experimental study and applications to dehydration and partial melting in the middle crust, *J. Petrol.*, 2014a, vol. 55, pp. 2419–2456.
- Safonov, O.G., Kovaleva, E.I., Kosova, S.A., et al., Experimental and petrological constraints on local-scale interaction of biotite–amphibole gneiss with H₂O–CO₂–(K, Na)Cl fluids at middle-crustal conditions: example from the Limpopo Complex, South Africa, *Geosci. Front.*, 2012, vol. 3, pp. 829–841.

- Safonov, O.G., Tatarinova, D.S., van Reenen, D.D., et al., Fluid-assisted interaction of peraluminous metapelites with trondhjemitic magma within the Petronella shear-zone, Limpopo Complex, South Africa, *Precambrian Res.*, 2014, vol. 253, pp. 114–145.
- Santosh, M., Carbonic metamorphism of charnockites in the southwestern Indian Shield: a fluid inclusion study, *Lithos*, 1986, vol. 19, pp. 1–10.
- Shmulovich, K.I. and Graham, C.M., Melting of albite and dehydration of brucite in H₂O–NaCl fluids to 9 kbars and 700–900°C: implications for partial melting and water activities during high pressure metamorphism, *Contrib. Mineral. Petrol.*, 1996, vol. 124, pp. 370–382.
- Shmulovich, K.I. and Graham, C.M., An experimental study of phase equilibria in the systems H₂O–CO₂–CaCl₂ and H₂O–CO₂–NaCl at high pressures and temperatures (500–800°C, 0.5–0.9 GPa): geological and geophysical applications, *Contrib. Mineral. Petrol.*, 2004, vol. 146, pp. 450–462.
- Sisson, T.W., Ratajeski, K., Hankins, W.B., and Glazner, A.F., Voluminous granitic magmas from common basaltic sources, *Contrib. Mineral. Petrol.*, 2005, vol. 148, pp. 635–661.
- Skjerlie, K.P. and Douce, A.P., Anatexis of interlayered amphibolite and pelite at 10 kbar: effect of diffusion of major components on phase relations and melt fraction, *Contrib. Mineral. Petrol.*, 1995, vol. 122, pp. 62–78.
- Srikantappa, C. and Zargar, S.A., First report on the halite-bearing fluid inclusions in the Precambrian granulites around Halaguru, Dharwar Craton, India, *Ind. Mineral.*, 2009, vol. 43, pp. 77–80.
- Touret, J.L.R., Fluid regime in southern Norway: the record of inclusions, The Deep Proterozoic Crust in the North Atlantic Provinces, *Proc. NATO Adv. Study Inst. Ser.*, 1985, vol. C158, pp. 517–549.
- Touret, J.L.R. and Huizenga, J.M., Fluids in granulites, *Origin and Evolution of Precambrian high-grade terrans, with special emphasis on the Limpopo Complex in Southern Africa*, Van Reenen D.D., Kramers J.D., McCourt S., and Perchuk L.L., Eds., *Geol. Soc. Am. Mem.*, 2011, vol. 207, pp. 25–37.
- Touret, J.L.R. and Nijland, T.G., Prograde, peak and retrograde metamorphic fluids and associated metasomatism in upper amphibolite to granulite facies transition zones, in *Metasomatism and the Chemical Transformation of Rock*, Berlin–Heidelberg: Springer, 2013, pp. 415–469.
- Tropper, P., Manning, C.E., and Harlov, D.E., Solubility of CePO₄ monazite and YPO₄ xenotime in H₂O and H₂O–NaCl at 800°C and 1 GPa: implications for REE and Y transport during high-grade metamorphism, *Chem. Geol.*, 2011, vol. 282, pp. 58–66.
- Tropper, P., Manning, C.E., and Harlov, D.E., Experimental determination of CePO₄ and YPO₄ solubilities in H₂O–NaF at 800°C and 1 GPa: implications for rare earth element transport in high-grade metamorphic fluids, *Geofluids*, 2013, vol. 13, pp. 372–380.
- Tsunogae, T., Santosh, M., and Shimpo, M., Sodic gedrite in ultrahigh-temperature Mg–Al-rich rocks from the Palghat–Cauvery shear zone system, southern India, *J. Mineral. Petrol. Sci.*, 2007, vol. 102, pp. 39–43.
- van Reenen, D.D., Hydration of cordierite and hypersthene and a description of the retrograde orthoamphibole isograd in the Limpopo Belt, South Africa, *Am. Mineral.*, 1986, vol. 71, pp. 900–915.
- van Reenen, D.D., Smit, C.A., Perchuk, L.L., et al., Thrust exhumation of the Neoproterozoic ultrahigh-temperature southern marginal zone, Limpopo Complex: convergence of decompression–cooling paths in the hanging wall and prograde *P–T* paths in the footwall, *Geol. Soc. Am. Mem.*, 2011, vol. 207, pp. 189–212.
- Vielzeuf, D. and Montel, J.M., Partial melting of metagreywackes. Part I. Fluid-absent experiments and phase relationships, *Contrib. Mineral. Petrol.*, 1994, vol. 117, pp. 375–393.
- Visser, D., Nijland, T.G., Lieftink, D.J., and Maijer, C., The occurrence of preiswerkite in a tourmaline–biotite–scapolite rock from Blengsvatn, Norway, *Am. Mineral.*, 1999, vol. 84, pp. 977–982.
- Watson, E.B. and Brenan, J.M., Fluids in the lithosphere, 1. Experimentally determined wetting characteristics of CO₂–H₂O fluids and their implications for fluid transport, host-rock physical properties, and fluid inclusion formation, *Earth Planet. Sci. Lett.*, 1987, vol. 85, pp. 594–615.
- Webster, J.D., Exsolution of magmatic volatile phases from Cl-enriched mineralizing granitic magmas and applications for ore metal transport, *Geochim. Cosmochim. Acta*, 1997, vol. 61, pp. 1017–1029.

Translated by E. Kurdyukov